Thesis for the Master's degree

# Filtration behavior of graphene oxide membrane with size-differentiated nanoflake and desalination performance enhancement by atomic layer deposition


Advisor : Professor, Kyu-Jung Chae

Feb. 2020

Graduate School of Korea Maritime and Ocean University
Department of Civil & Environmental Engineering
Tae-Nam Kim

Accepted in partial fulfillment of the requirements for the Master's degree

Committee member : Prof. Young-Chae Song _____

Committee member : Prof. Myoung-Jin Kim _____

Committee member : Prof. Kyu-Jung Chae _____

Jan, 09. 2020

Graduate School of Korea Maritime and Ocean University

# Table of contents

# List of Figures

# Abbreviations

ALD, atomic layer deposition

EDS, energy dispersive X-ray spectroscopy

FT-IR, Fourier-transform infrared spectroscopy

FE-SEM, field-emission scanning electron microscope

GO, graphene oxide

NF, nanofiltration

MD, molecular dynamics

RO, reverse osmosis

WCA, water contact angle

XRD, X-ray diffraction

XPS, X-ray photoelectron spectroscopy

# Filtration behavior of graphene oxide membrane with size-differentiated nanoflake and desalination performance enhancement by atomic layer deposition

Tae-Nam Kim

Department of Civil & Environmental Engineering
Graduate School of Korea Maritime and Ocean University

## Abstract

Multi-layered GO membrane (GOM) that is composed of atomic thick (0.34nm) graphene oxide (GO) flakes are mostly studied by researchers due to its unique water transport system, high chemical and mechanical stability. However, their low salt rejection efficiency and significant decrease of water permeability limit their wide application in water desalination. This research aims to understand the water transport mechanism and enhancing GOM performance. To investigate GOM behavior during filtration, GOMs composed with different sized GO flakes were applied. Moreover, on the purpose of enhancing water purification performance, a novel surface nano-functionalization method, atomic layer deposition (ALD) was applied. It was observed that water molecule transportation through GOM is limited by enveloped region where edge

and basal plane of each GO meets. Interlayer space of wet state GOMs by X-ray diffractometer revealed that smaller GO stacked membrane possesses more enveloped region. Due to the narrowed nanochannel of GOM, water filtration with larger GO stacked GOM showed two folds higher permeability than GOM containing smaller GO nanoflakes. This study suggests that any modification of GOM that could affect the microstructure of membrane should consider such invariance of structural defects of GOM. ALD allowed for the formation of an ultra-thin $Al_2O_3$ layer (1.44nm) on the surface of GOM, due to the strong chemisorption of $Al_2O_3$ precursor, trimethylaluminum to GO. Atomically thin coating of $Al_2O_3$ layer enhanced water permeability (from 40LMH/bar to 75LMH/bar) and NaCl rejection up to 67.4%, overcoming the trade-off between permeability and selectivity. This enhanced filtration performance is mainly attributed to the changes of surface electrochemical properties without affecting the GOM microstructure. X-ray diffraction, X-ray photoelectron spectroscopy, Fourier-transform infrared spectroscopy and water contact angle were performed to investigate the effect of ALD on the physico-chemical properties of GOM. The distinctive features of ALD to the GO membrane may contribute towards enhancing its wider application in water desalination.

**Key words**: Graphene Oxide, Graphene Oxide Size, Atomic Layer Deposition, Salt Rejection, Membrane Technology, Water Desalination

# 산화그래핀 여과막의 물여과 특성 평가 및 여과성능 향상을 위한 원자층증착법의 적용

김 태 남

한국해양대학교 대학원
토목환경공학과

**초록**

최근 2차원 탄소계 물질인 그래핀옥사이드(graphene oxide, GO)가 차세대 여과막 소재로 각광받고 있다. GO는 두께가 탄소분자 1개 원자층(0.34nm) 정도로 매우 얇고, 탄소원자간 $sp^2$ 결합으로 인해 화학적으로 매우 안정하며 산소계 작용기(-OH, COOH 등)의 작용으로 매우 친수성을 가진다. 하지만 GO 나노입자의 높은 친수성으로 인해 물 여과 시 내부 구조가 수화하여 염 제거율이 ~50%정도로 매우 낮아진다. 더불어, 수화된 GO 여과막은 물 여과 시 구조가 압밀화(compaction)되어 수 시간동안 초기 물 투과율 대비 10%수준으로 감소하는 현상이 최근 발견되었다. 본 연구에서는, 1. 물 여과시 GO 나노여과막의 내부 구조 특성 파악을 위해 서로 다른 입자의 GO 나노입자를 적층한 나노여과막을 제작하여, 여과막 내부 구조 특성 및 여과성능을 평가하였고 2. 여과막 표면을 나노수준으로 개질할 수 있는 원자층증착법(Atomic layer deposition, ALD)을 적용하여 담수화 성능을 평

가하였다. GO 나노입자의 크기가 작을수록 GO 여과막의 내부층 나노채널의 크기가 감소하고 균일도가 높게 관찰됨을 XRD를 통해 확인하였다. 여과막의 압밀화현상에 의한 여과율 감소는 나노입자가 가장 큰 여과막이 제일 적게 나타났으며, 투과율이 안정화 된 상태에서 측정한 물 투과율은 큰 입자로 이루어진 여과막이 16.6kg/$m^2$hr/bar, 작은 입자로 이루어진 여과막은 8.4kg/$m^2$hr/bar로 약 2배의 차이를 보였다. 표면을 나노단위 수준으로 코팅하는 원자층증착기술을 통해 GO 여과막에 $Al_2O_3$가 증착두께 0.16nm/ALD cycle로 증착됨을 확인하였으며, ALD에 의해 GO 여과막의 표면이 산소계 작용기로 개질됨을 XPS와 FT-IR을 통해 확인하였다. 물 투과율과 염 제거율이 동시에 증가함을 관찰하였다. ALD를 9번까지 증가시킨 GO 여과막은 NaCl 제거율이 기존 40% 대비 67%로 약 2배 증가하였으며 물 투과율 또한 40LMH/bar에서 75LMH/bar로 증가하였다. 이와 동시에 ALD 에 따른 GO 여과막의 내부구조 변화와 여과막의 손상은 발생하지 않음을 XRD와 Raman을 통해 확인하였다.

**주제어**: 그래핀옥사이드, 그래핀옥사이드 여과막, 원자층증착법, 염 제거, 여과막 기술, 담수화

# Chapter 1. Introduction

Membrane filtration technology is one of the most effective solution for clean water production. As demand of clean water increased, various membrane technology has been developed based on membrane pore size tuning (from microfiltration to reverse osmosis), osmotic pressure application (forward osmosis and pressure retarded osmosis) over past centuries. The most important compartment of membrane filtration technology is semipermeable membrane where pollutants (ion, suspended solids, heavy metal, etc.) are separated from water. The most widely used membrane is composed of polymers due to their relatively cheap price and feasibility to meet required pollutants removal efficiency from water. The dominant factor affecting pollutant removal efficiency and total operational considerations is pore size of semipermeable membrane. For this reason, membranes are classified into four types, microfiltration (MF), ultrafiltration (UF), nanofiltration (NF) and reverse osmosis (RO). As illustrated in Fig. 1.1, each type of membranes are used to meet required water quality.

Up to date, polymeric membrane is world-widely selected for all classification of membranes due to their relatively cheap price and feasibility to fabricate and modify to meet their needs. However, polymeric membranes possess limitations on chemical and mechanical stability. Especially, when it comes to desalinate seawater, chemical degradation of NF and RO membranes by chlorinated compounds from pre-treatments of filtration limits its sustainability (Avlonitis et al., 1992). Such chlorination of polymeric membranes (i. e., polyamide, cellulose acetate) accelerates the hydrolysis, consequently, unwanted defects

occurs where salts and solids penetrate the membrane.

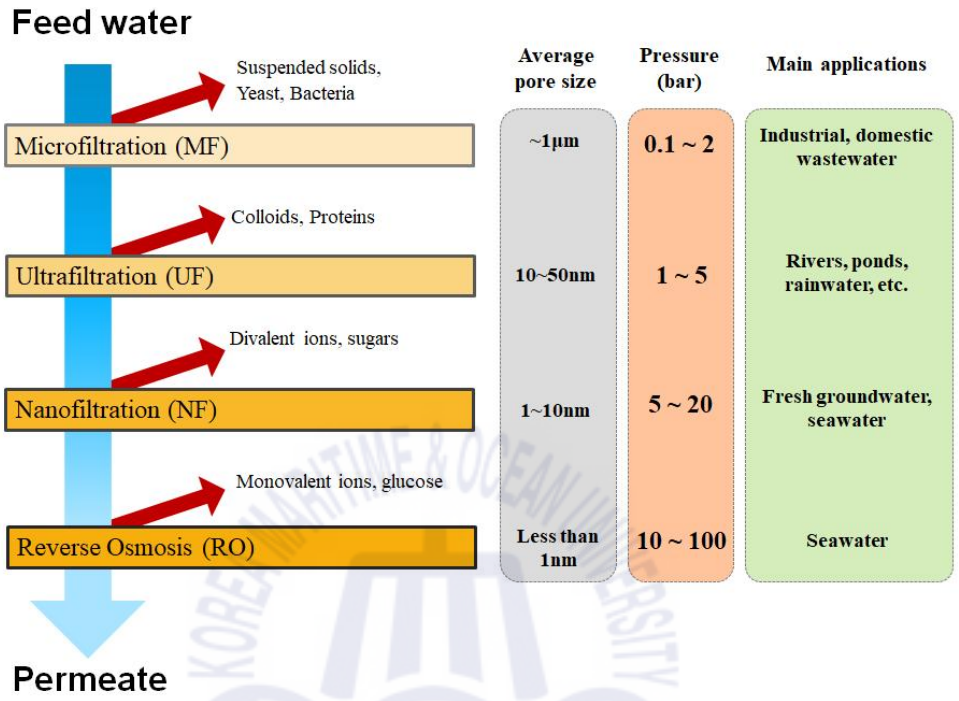


Fig. 1.1. Classification of semipermeable membranes by pore size

To overcome the existing membrane challenges, new class of carbonic nano-material, graphene oxide (GO), which is single layer of highly oxidized graphite is recently studied for water filtration membrane (Anand, A. et al, 2018; Zheng, S. et al, 2017, MI, B. et al., 2018). Due to the various oxygen containing functional groups on the two-dimensional (2D) structure with the thickness of around 1nm, the GO laminate becomes hydrophilic that is advantageous in water filtration. Moreover, carbonic $sp^2$ bonds of single GO nanoflake exhibits extremely strong chemical stability. Most popular form of GO membrane (GOM) used for water filtration is laminarly stacked GO laminates where 2D laminar interlayer space between adjacent GO nanosheets act as major water

pathway.

To successfully desalinate water, the size of interlayer space of GOM for ion sieving from water should reach less than 7Å to reject hydrated sodium (Na+, with a hydrated radius of 3.6Å) from water (Dayer, D. R. et al., 2010). However, due to the elastic and hydrophilic nature of GO nanoflake, nanochannel size dramatically increase to 15Å. Such swelling behavior of GOM under wet state exhibits around 50% of NaCl rejection during filtration (Mohammad, A. W. et al., 2015).

Various efforts have been attempted to overcome such issues of ion-sieving GOMs. Researchers have applied polymers to cross-link agents between adjacent GO nanoflakes via covalent bonding polymers (Kim, S. et al., 2018). As a result, polymer loading inhibited the swelling of the GOM hence showing improved salt rejection. However, narrowed interlayer space resulted in a significant decline in water permeability, 71.2% and 74.8% for deionized (DI) water and salt water, respectively. Another modification of GOM aimed to reduce the interlayer space by the chemical reduction of oxygen-functional groups of GO (Yang, E. et al., 2017). To complement the reduced permeability, additional polydopamine (pDA) coating was performed on the surface of GOM by PDA solution. This PDA coating layer improved the efficiency of rejecting pollutants, but decreased water permeability due to the increased membrane thickness.

Very recently, dramatic and continuous flux decrease during pressurized GOM filtration process is reported by (Chong, J. Y. et al., 2018). The authors state that flux declined to 10% of its initial flux after 12 hours of filtration due to the compaction of interlayer space of adjacent GO. To our best knowledge, there has been no researches fully

discuss about this issue yet.

In conclusion, aforementioned issues of low salt rejection and continuous water flux decline rely on the understanding of microstructure of GOM. (Klechikov, A. et al., 2015; Talyzin, A. V. et al., 2014) declared that unlike parallelled 2D nanochannel of GOM, actual GOM microstructure consists of disorders due to the elasticity of GO so that careful considerations on modification of GOMs should be performed.

In this study, microstructural behavior during water filtration by GOM is investigated by differentiating GO nanoflake size to find a microstructural factor that influences the filtration performance of GOM. It is reported in (Klechikov, A. et al., 2015) that current GOM structure is over simplified that hinders the actual dynamics of water fluids within GO nanoflakes. Our hypothesis is that GOM with smaller GO stacked membrane may form such denser structure when pressurized than that of larger GO stacked one. Then, GOM is modified to develop salt rejection and water filtration performance via unique coating method that functionalizes the surface of substrate by sub-nanometer level, atomic layer deposition (ALD). As mentioned above, such coating methods decrease the membrane filtration performance because of increased membrane thickness and structural disorders occurrence during the modification. There are a few cases of applying ALD to membrane functionalization. However, Via ALD is a process that coating is processed under dry condition with relatively low temperature (50~150℃).

# Chapter 2. Literature review

## 2.1 GO membranes behavior during water filtration

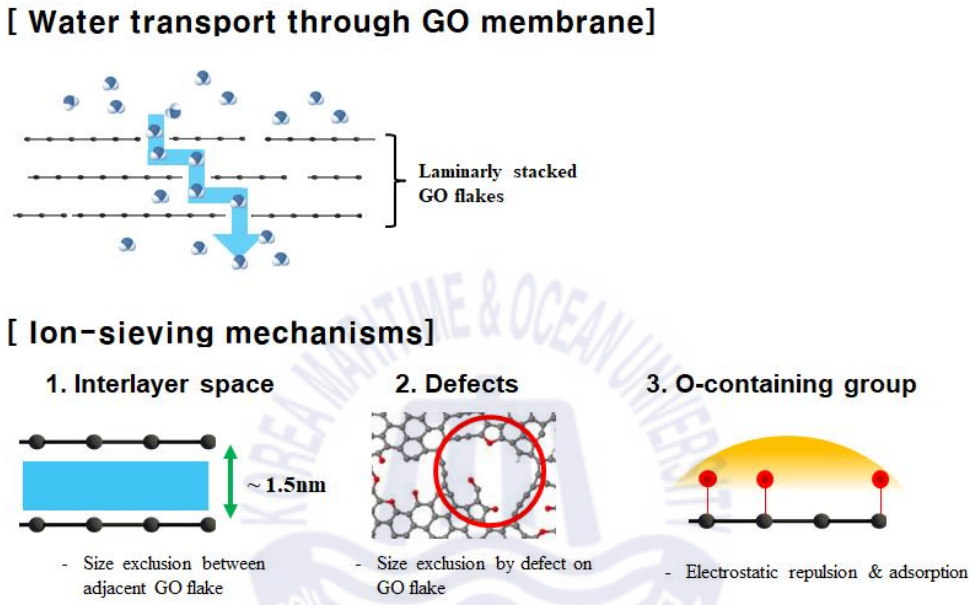


**Fig. 2.1.** Water transport and ion (salt) sieving mechanisms of multi-layered GO membrane

There are three major mechanisms of ion-sieving by GOM as illustrated in Fig. 2.1, size exclusion via interlayer space, defect on GO nanoflake and electrostatic repulsion between ions and oxygen containing functional groups on GOM. As mentioned in chapter 1, interlayer space is governing factor that influences both water permeability and ion rejection efficiency. In case of multi-layered GOM, interlayer space between laminarly stacked GO nanosheets is regarded as one of the most important factor on filtration performance (Yang, E. et al., 2018; Nair, R. R. et al., 2012; Zheng, S. et al., 2017; Zhao, Y. et al., 2016;

Kim, S. et al., 2018; Huang, L. et al., 2015; Mi, B. et al., 2018).

Up to now, as proposed by (Nair, R. R. et al., 2012), length of GO nanoflake hinders the water permeability as larger GO nanosheet provides longer pathway through GO stacked layers. Currently applied GOM permeability calculation model is classic Hagen-Poiseuille (H-P) equation, considering the size of GO flakes as tortuosity, as well as interlayer space as pore size and membrane thickness. However, H-P and other related calculation models over-simplify the GOM microstructure that such perfect laminar structure is impossible to be made especially during the mostly used solution-based GO stacking process. In (Chong, J. Y. et al., 2018), water flux was calculated with various membrane thickness and size of GO conditions. It was revealed that even by reducing the GOM thickness by 20nm, calculated flux was hundreds of magnitude lower than experimental results.

To fully understand the aforementioned significant decrease of flux during filtration, it is noteworthy to address that the microstructure of GOM is imperfect laminar structure thus may exhibit changes during the filtration.

## 2.2 Atomic layer deposition on GO membrane

Unlike conventional coating methods, such as layer-by-layer, chemical vapor deposition (CVD) and vapor-based coating, ALD is a fascinating dry-state coating that enables precise atomic level thickness control (George, S. M. et al., 2010). While, the CVD process forms a thin film through a chemical reaction at temperature level of several hundreds, ALD forms a atomic thin layer through self-limiting reaction between surface of substrate and injected precursor. The unit ALD cycle consists

of four steps, [precursor injection] - [precursor purge] - [reactant pulse] - [reactant purge] as depicted in Fig. 2.2. Since the precursor and reactant are injected separately in few seconds and space through the purge step in the ALD process, only the chemi-sorbed precursors to the substrate can be converted into a thin film. If the injection times of each step are sufficient for saturation, the deposited layer thickness per one cycle is constant and is called a self-limiting growth characteristic. Therefore, a thin film deposited using ALD can be deposited with sub-nanometer thickness by controlling its unit cycle. In this regard, ALD can be a novel method for surface modification of membranes and in various membrane technologies.

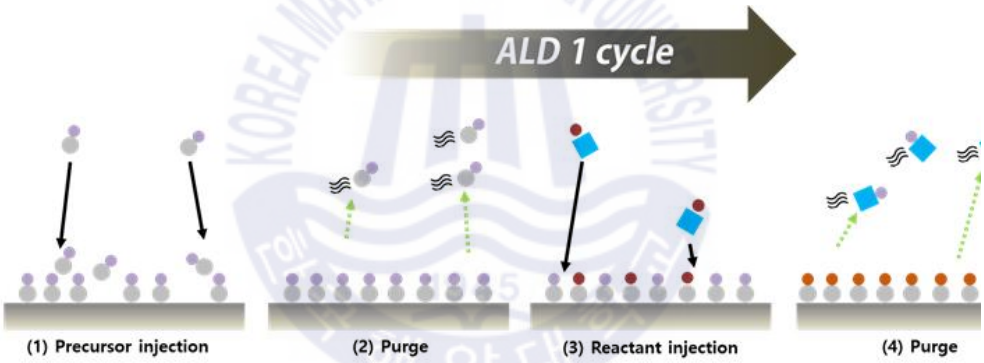


Fig 2.2. Schematic illustration of ALD process

Recently, plasma-enhanced ALD (PEALD) that uses oxygen radicals as a reactant, can deposit a metal oxide layer at lower temperatures than thermal ALD (George, S. M. et al., 2010). Leveraged by it, PEALD method have been used to functionalize membrane surfaces in order to engineer physico-chemical properties of the membranes (Li, F. et al., 2011). It is reported that after the range of 10-600 PEALD cycles, uniformly deposited metal oxides tuned the pore size and thickness precisely, hence increased hydrophilicity, and decreased surface

roughness, which significantly contributed to favorable pollutant rejection efficiency and inhibition of biofouling on the surface of membranes (Nikkola, J. et al., 2014; Li, N. et al., 2018).

Up to date, ALD method are only focused on the increasing separation efficiency by tuning size exclusion and hydrophilicity for flux enhancement. Moreover, in order to facilitate the advantageous properties of ALD, a few ALD cycles has to be performed to minimize the ALD modification time and to prevent flux decline due to the increased membrane thickness.

ALD has been applied as a method for healing defects on 2D carbon nanomaterials (Van Lam, D. et al., 2014; Wang, X. et al., 2008; Kim, K. et al., 2014). As such, the application of ALD to multi-layered GOM could result in defect-free membranes without losing its hydrophilic surface. Zhou (2018) implied that only a few cycles of ALD on a polymeric NF membrane is desired because ALD blocks the water entrance pores (Zhou, X. et al., 2018). Aluminum oxide ($Al_2O_3$) is the representative metal oxide for the ALD process. Due to its high exothermicity and excellent affinity to oxygen-functionalized region of GO, $Al_2O_3$ has advantageous features of conformal deposition with minimal surface roughness over the entire temperature range of ALD with minimal change in the growth per cycle (Groner, M. D. et al., 2004; Nourbakhsh, A. et al., 2015).

# Chapter 3. Materials and methods

## 3.1 Size-differentiated GOM fabrication

The fabrication procedure of the GO membrane with different GO sheet size is summarized in Fig. 3.1. First, to obtain the GO layered (stacked) structure, a high concentration of GO solution (10 mg/mL, Tokyo Chemical Industry, Japan) was diluted to 0.005 mg/mL with DI water. To differentiate the size of GO nanosheets, we used physical destruction method, probe-type sonication for 1 hour with different sonication energy, 55, 165 and 275W, respectively. During the sonication, as-prepared GO solution were stored in a beaker which is soaked in sonication bath filled with water to prevent thermal reduction during sonication procedure. After sonication, GO laminate was deposited on the commercial mixed cellulose ester membrane with a pore size of 0.2 $\mu$m (47mm area, ADVANTEC, Japan) by vacuum filtration. After GO deposition, all membrane samples were dried in a desiccator overnight prior to filtration test and characterization.

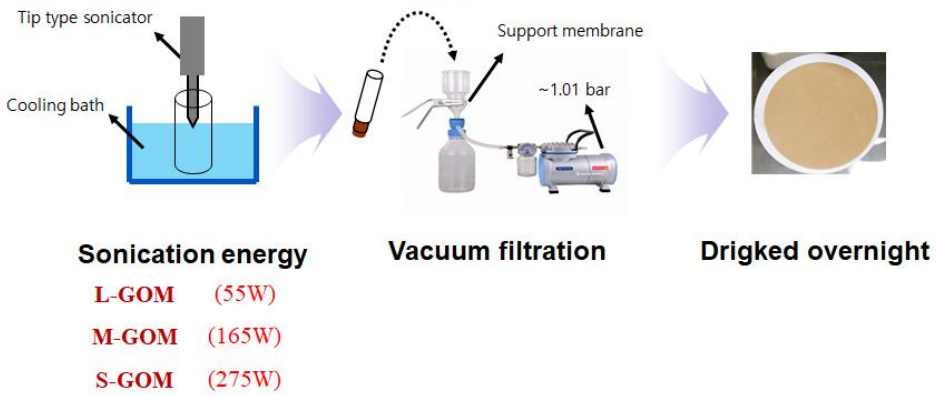


**Fig. 3.1** Fabrication process of GO size-controlled membrane

### 3.2 Surface modification of GOMs by ALD

The fabrication procedure of the ALD-$Al_2O_3$@GO membrane is described in Fig. 3.2. First, 165W sonicated GOM was kept in desiccator for one day before ALD process. The ultra-thin $Al_2O_3$ layer was obtained on the prepared GO membrane using a 6-inch PEALD reactor (iOV d150, iSAC Research, Korea). For the $Al_2O_3$ layer deposition, TMA was used as the aluminum source and the entire process was conducted at a temperature of 140℃ under 1 Torr of pressure. A PEALD cycle for $Al_2O_3$ layer deposition proceeded with the following four steps: TMA precursor feeding (0.5sec), argon (Ar) purging (5sec), oxygen ($O_2$) plasma (3sec), and Ar purging (10sec), which was the saturation condition. The Ar purging step was conducted to avoid unwanted reactions between products/by-products ($Al(CH_3)_2/CH_4$) of the feeding step and $O_2$ plasma step. Then, the $O_2$ plasma step, which is used as a reactant to transform adsorbed trimethylaluminum ($Al(CH_3)_2$) into $Al_2O_3$ on the GO membrane, was conducted with a power of 200 W. Another purging step was undertaken to remove water ($H_2O$), carbon dioxide ($CO_2$), and carbon monoxide (CO), which are by-products of the combustion-like reaction between $Al(CH_3)_2$ and $O_2$ plasma.

### 3.3 Membrane characterization

#### 3.2.1 Phyiso-chemical properties of GO nanoflake and GOMs

Size of GOM nanoflakes was evaluated by particle size analyzer (PSA) and UV-Vis, (Mastersizer 3000E, Malvern, UK). By PSA, both mean size and size distribution of as-prepared GO solutions and untreated GO solution were compared. Furthermore, intensity of UV-Vis peak at 230nm was compared between each sonicated GO samples to support the size

variation. Raman spectroscopy (NRS-5100, Jasco, Japan) was utilized to evaluate the structural defects during probe-type sonication process to GO nanoflakes. Defect on each GO membrane surface was calculated as follows (1):

$I_D/I_G$ =(Intensity of D peak)/(Intensity of G peak), (1)

### 3.2.2 Water intercalation behavior inside the GOMs

To obtain microstructural properties of each membranes under both dry-state and wet-state, X-ray diffraction (XRD, Smartlab, Rigaku, Japan) was conducted by 2-theta mode ranging from 5° -20° with Cu K$\alpha$ radiation. Full-width half maximum (FWHM) was obtained for each XRD spectra to investigate nanochannel size distribution. Size of 2D nanochannels between GO flakes were calculated using the following Bragg's equation (2):

$\lambda = 2d \times \sin\theta$, (2)

where $\lambda$ is the X-ray beam wavelength of Cu K$\alpha$ radiation (1.5406 Å), d is the interlayer space between stacked GO flakes, and $\theta$ is the diffraction angle.

### 3.2.3 Confirmation of ALD-$Al_2O_3$ deposition on the surface of GOM

Confirmation of ALD-$Al_2O_3$ deposition on the GO membrane surface was observed by combining Field Emission Scanning Electron Microscopy (FESEM, MIRA3 LMH, Tescan, Czech Republic) and Energy Dispersive Spectroscopy (EDS). The chemical structure of the membrane surface was examined by Fourier-transform infrared spectroscopy (FTIR, Spectrum GX, Perkin Elmer, USA) and X-ray photoelectron spectroscopy (XPS, Multi2000, Thermo VG Scientific, UK). The FTIR spectra were

measured.

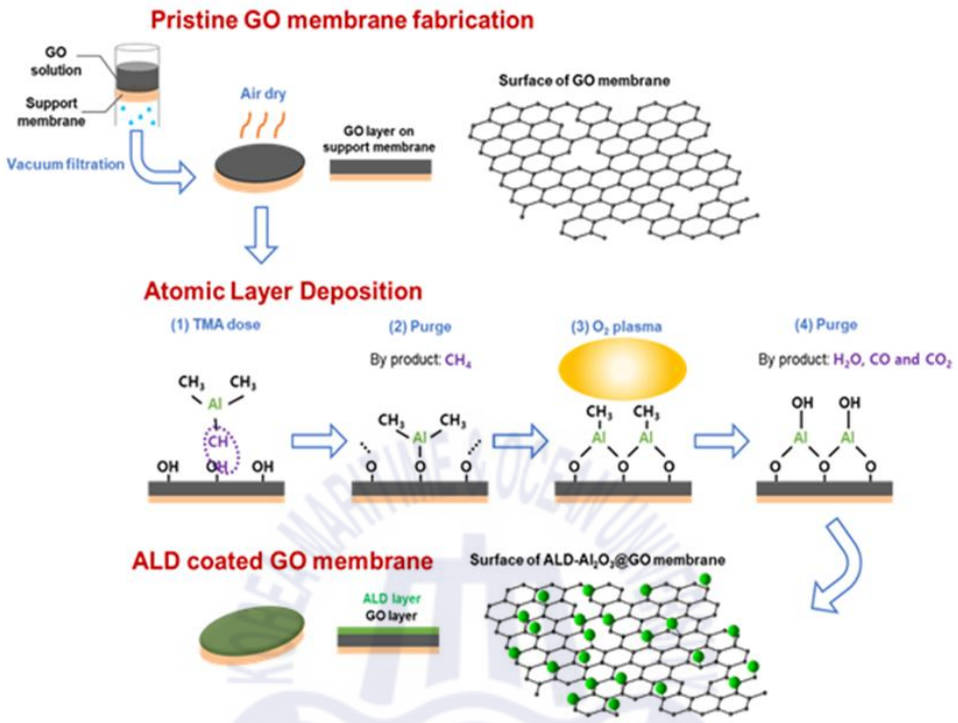


**Fig. 3.2.** Schematic illustration of ALD coating process on GOM

in attenuated total reflection mode, wavelength range from 700cm-1 to 4000cm-1. XPS analysis was conducted for both survey scan and high-resolution C1s and O1s scan with step size of 1.00eV and 0.025 eV, respectively. Carbon oxygen ratio (C/O) was calculated as atomic concentration of carbon ($C_{at.\%}$) divided by that of oxygen ($O_{at.\%}$) as described in (3),

$$C/O=(C_{at.\%})/(O_{at.\%}), \quad (3)$$

where Cat.% and Oat.% are the atomic concentration of carbon and oxygen, respectively.

### 3.2.4 Physico-chemical properties of ALD coated GOM

Contact angle measurements were carried out using a 6 uL sessile droplet of Milli-Q water with a Krüss Easy Drop goniometer. Each point at different locations on the same as-prepared membrane samples was measured and averaged. X-ray diffractometer (XRD) measurements in the 2-theta mode ranging from 5° -20° were performed using copper-potassium-alpha (Cu K$\alpha$) radiation to measure the nanochannel size of the GO membrane and ALD-$Al_2O_3$@GO membrane samples.

Raman spectroscopy was aquired to investigate the effect of ALD on GO structural defects behavior. The thickness of $Al_2O_3$ layers for 3, 6, and 9 cycles were evaluated by the growth rate of the deposited layer with increasing ALD cycles. First, the thicknesses of $Al_2O_3$ layers were measured by an Ellipsometer (Elli-SE, Ellipso Technology) using deposited samples on a silicon (Si) substrate. The growth rate under saturated conditions was extracted from the slope of the linear extrapolation of the graph. Subsequently, the thickness of the ultra-thin $Al_2O_3$ layers under 3, 6, and 9 cycles was calculated as follows (4):

Thickness = Number of cycles × Growth rate, (4)

### 3.3 Membrane filtration performance evaluation

Pure water and salt water permeability were evaluated in a high-pressure dead-end filtration cell (HP4750, Sterlitech, USA) under 5 bar at room temperature. For both DI water and salt water permeability, the amount of permeates was weighed using a nimbus precision balance equipped with ADAM DU software (Adam Equipment, USA). First, 100 mL of DI water was filtered through the inserted membranes to obtain DI water permeability. Subsequently, 100 mL of salt water (2000 mg/L of NaCl) was filtered to measure the NaCl solution permeability and NaCl rejection. The permeability (LMH/bar), was calculated by the following

equation:

$$\text{Permeability} = V/(A \times t \times P), \quad (5)$$

where V is the volume of the permeate (L), t is permeation time (h), A is the effective membrane area of the membrane (14.6 $cm^2$) and P is applied pressure to membranes.

NaCl rejection efficiency R was obtained by the following (6):

$$R(\%) = (C_f - C_p)/C_f \times 100, \quad (6)$$

where $C_p$ and $C_f$ are permeate and feed concentrations, respectively. The salt concentration of the permeates was measured with inductively coupled plasma (ICP, Optima 300DV, PerkinElmer, USA) to evaluate salt rejection of the membrane samples.

# Chapter 4. Results and discussion

## 4.1 Physico-chemical properties of controlled size GO flakes

Prior to investigate the effect of GO nanoflakes on microstructural behavior of GOM, we first evaluated the size differentiation of sonicated GO. Fig. 1 illustrates the decrease of GO mean size obtained by PSA. As can be seen, all GO solution with probe-type sonication treated showed mean size of less than 1㎛ while average size of untreated GO sample was 5.75㎛. It is in good accordance with (Chen, J. et al., 2015; Le, G. T. T. et al., 2019; Xia, M.-Y. et al., 2019) that the use of probe-type sonication is an effective tool to breakdown GO flakes with. As depicted in Fig. 4.1 inset graph, continuous decrease of GO nanosheet size was observed when sonication energy got increased showing 0.835, 0.558 and 0.478㎛ for L-GOM, M-GOM and S-GOM. Compared to the degree of size decline between sonication treated and untreated GO sample, increase of sonication energy by 5 times (55W and 275W) exhibited size changes for sub-micrometer (L-GOM and S-GOM). According to (Gonçalves, G. et al., 2014), higher sonication energy is required to obtain smaller GO sheets, especially when the GO size is nanolevel.

We performed UV-Vis to support the size distribution from PSA analysis (Fig. 2). UV-Vis is a promising tool to investigate structural properties (i.e., $sp^2$ and/or $sp^3$ bond) of carbonic materials. Recently, (Zhang et al., 2019) reported that UV-Vis intensity showed proportional relationship with size of GO flakes. As can be seen from Fig. 4, higher absorbance peak at 230nm was observed for higher sonication energy

applied that is in good agreement with (Zhang, T. et al., 2019; Xia, M.-Y. et al., 2019). Regarding the decreased mean GO size and higher absorbance peak by PSA and UV-Vis, destruction of GO sheets was confirmed as a function of probe sonication energy.

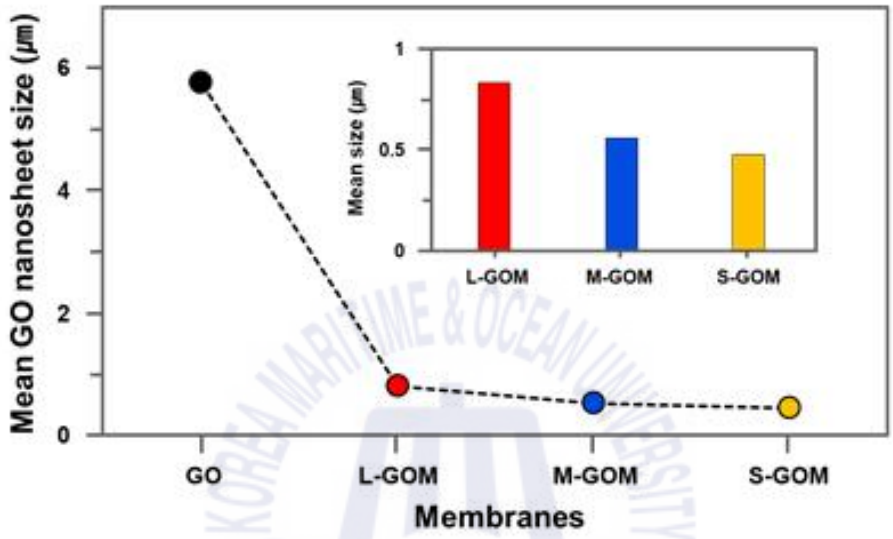


Fig. 4.1. Changes of GO mean sizes with untreated GO and probe-type sonication treated GO samples (inset graph)

Fig. 4.3 shows the size distribution of each GO samples. The untreated GO exhibited a broad size distribution, varying from less than 1㎛ to maximum 100㎛. The use of probe-type sonication effectively narrowed the size distribution of GO sizes, showing less size variance than 10㎛ which is in good accordance early studies (Huang, D. et al., 2019; Shen, B. et al., 2012). However, no significant distribution homogeneity change was found for sonication energy.

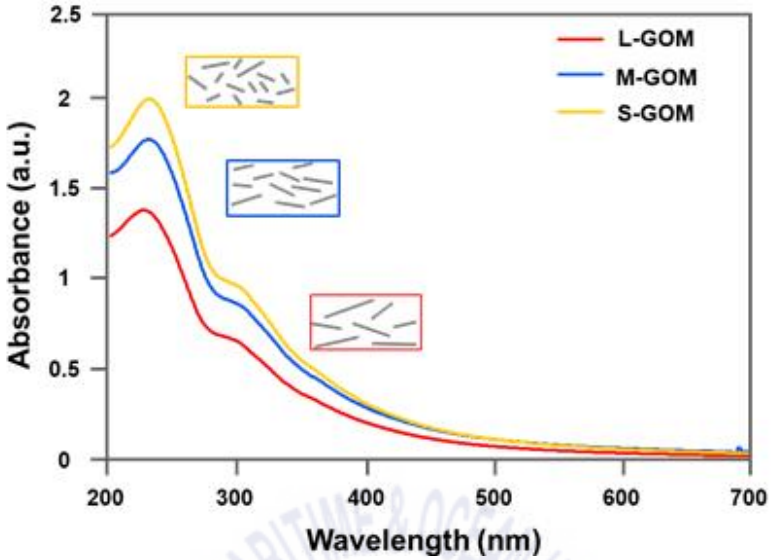


Fig. 4.2. UV-vis spectra of sonicated GO solution with different sonication power

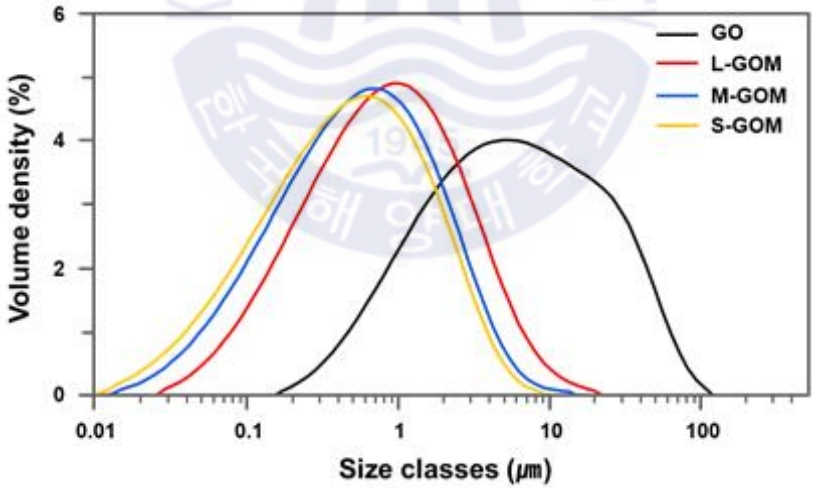


Fig. 4.3. PSA spectra for untreated and probe-type sonicated GO samples

We then acquired Raman spectra to investigate the sonication induced structural defects on basal-plane of GO nanosheets (Fig. 4.4). As is

known, defects on a graphene and its derivatives provide water molecule pathway through basal-plane (Boretti, A. et al., 2018; Qi, H. et al., 2018). Structural defect of GO nanosheet is usually studied by calculating ratio between intensity of D ($sp^3$) and G peak ($sp^2$) expressed as $I_D/I_G$ ratio (Shen, B. et al., 2012). As illustrated in Fig. 4, ID/IG ratio of all GOMs remained almost unchanged. Our Raman data confirms that molecules penetration through GOM will not be affected by carbonic structured defect for all GO samples.

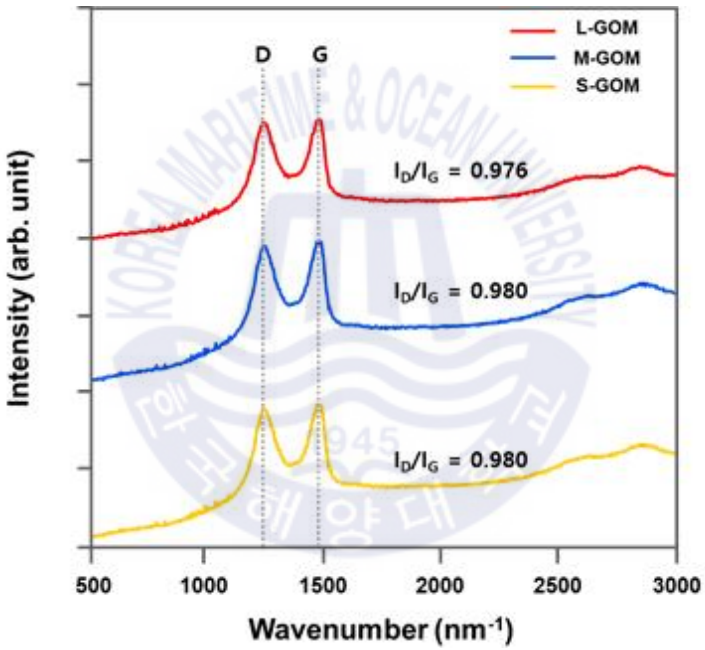


**Fig. 4.4.** GO defect analysis by Raman with different sonication power

It is of great interest to investigate how the inner microstructure (e.g., mean pore size, porosity and tortuosity) of the fabricated membrane shapes because it significantly influences the filtration performance of membranes. In case of multi-layered GOM, interlayer space between

laminarly stacked GO nanosheets is regarded as one of the most important factor on filtration performance (Yang, E. et al., 2018b; Nair, R. R. et al., 2012; Zheng, S. et al., 2017; An, D. et al., 2016; Huang, L. et al., 2015; Mi, B. et al., 2018; Moon, I. K. et al., 2010; Yang, E. et al., 2018a). As illustrated in Fig. 4.5b, enlargement of interlayer space was observed when the membranes are immersed in water. Increase of interlayer space of GOMs is due to the intercalation of water molecules between GOMs. Interlayer space under wet state was seemed to be proportional to the size of GO nanosheets, showing 18.4, 14.5, 13.8 and 13.6Å for pristine GOM, L-GOM, M-GOM and S-GOM, respectively. It should be noted that the dry state of all GOMs showed almost same nanochannel size (8.7Å), which is due to the oxygen containing groups of GO flakes resists adhering to each other (Stobinski, L. et al., 2014). Some reports investigated the change of interlayer space by controlling oxygen-containing functional groups on the GO via thermal reduction (Zhao, Y. et al., 2016; Dolbin, A. V. et al., 2016) and hydroiodic acid vapor (Yang, E. et al., 2018b) showed apparently different d(001) peak position.

To verify more detailed microstructural condition of each membrane, we further investigated structural disorders of GO microstructure via calculating width of d(001) peak. As can be seen in Fig. 4.5a and 4.5c, broad d(001) peak of wet state XRD spectra was shown for larger GO stacked membranes. The highest FWHM value of pristine GOM showed ~2.8 $\theta$ while sonication-fabricated membranes exhibited only 1.18, 0.91 and 0.87 $\theta$. Regarding that each theta of XRD spectra indicates the size of GO nanochannel, it can be discussed that the structural disorders occur more for larger GO stacked membranes.

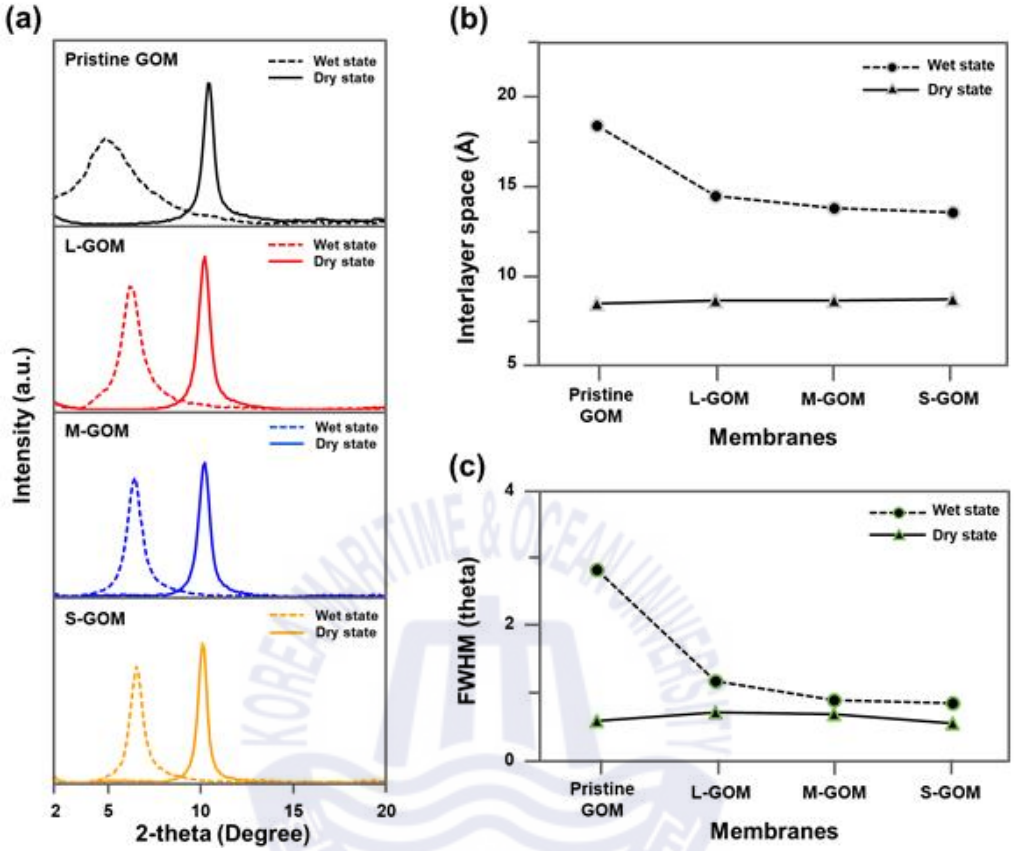


Fig. 4.5. Interlayer space measurement by XRD for fabricated membranes (a) XRD spectra for dry and wet state (b) interlayer space and (c) full-width half maximum (FWHM) comparison between each membranes

As mentioned above, it is discussed in early reports that the actual GOM microstructure is not a complete paralleled structure but the complex of disordered nanochannels due to different functionalities of GO edge and basal-plane (Chong, J. Y. et al., 2018, Talyzin, A. V. et al., 2014). During solution-based GO stacking process such as vacuum assisted filtration, repulsion of -OH that is dominantly decorated at the edge of GO flake between adjacent GO induces incomplete parallel stacking where edge and basal-plane encounters. (Klechikov, A. et al., 2015) reported that

aforementioned overlapping produces a kind of dead-end pore (the authors stated the term "enveloped" in the article) where molecules are suppressed to enter. In this regard, our XRD analysis results meets the Klechikov's results that larger GO stacking becomes more disordered structure than smaller GOM. There should be more basal-to-basal GO region where each GO nanoflakes faces each other laminarly for L-GOM than M-GOM and S-GOM, as the same amount of GO was loaded to membranes. This implies that water permeation through multi-layered GOM may be strongly hindered when water molecules pass through enveloped region.

### 4.2 Water transport through GOMs during water filtration

Membrane filtration performance was evaluated for as-prepared GOMs (Fig. 4.6). As expected, significant flux decrease was occurred for all GOMs during 6 hours of filtration. (Chong, J. Y., 2018) reported that such declination is due to the loosely packed microstructure in the early stage of filtration. Under the same filtration condition, L-GOM exhibited relatively smooth flux decline (Fig. 4.6a) than smaller GO stacked membranes. When GOM was first exposed to water before filtration, water transport driving force within nanochannels is governed by diffusion of water molecules that in the end induces complete delamination of GOM. In case of pressurized condition, water molecules rapidly penetrate through both edge-to-basal region and basal-to-basal region. In contrast to delamination of GOM, significant GO nanoflakes compaction occurs during water penetration through GOM. It can be explained by high adsorption interaction between GO and water molecules. As GO nanoflakes stacks to each other more closely, enveloped region is formed more under pressurized system.

Not just the compaction rate, but also the water permeability is declined when smaller GO flakes are stacked than the larger GO flakes. DI water permeability of last 1 hour of total period of filtration for L-GOM was 16.6kg/m$^2$hr/bar while S-GOM only achieved 8.4kg/m$^2$hr/bar (Fig. 4.6b). This low permeability can be also explained by high ratio of edge-to-basal S-GOM.

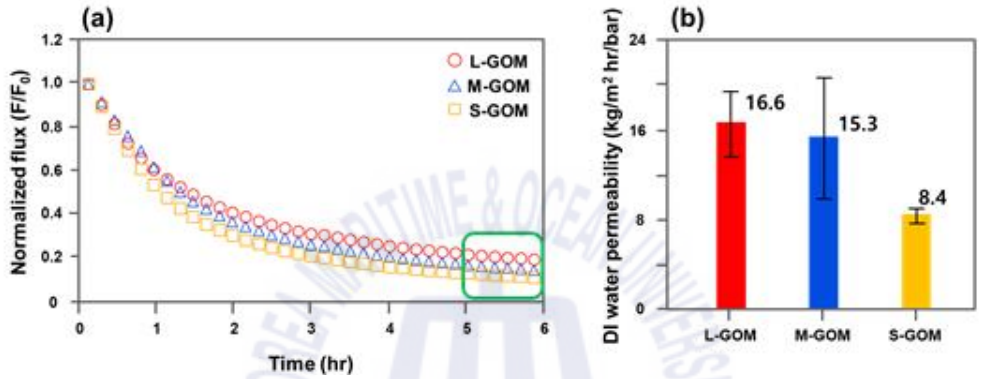


**Fig. 4.6.** GOMs filtration performance tests (a) normalized DI water flux ratio of initial flux to measured flux every 10 mins (b) permeability of last 1 hour of filtration (green box)

We then compared water flux of L-GOM and S-GOM under different pressure in Fig. 4.7. As expected, higher pressures exhibited high rate of flux decline for both membranes. It reflects that GOM compaction of basal-to-basal ratio is faster as water flows and drags GO nanoflakes to be more compacted. It is interesting to note that very small pressure (less than 1bar) will keep the microstructure almost unchanged. Regarding the energy consumption to obtain S-GOM that requires 5 times more energy than L-GOM, larger GO will be favorable to obtain more pure water. However, pollutants with different sizes such as humic acids, sugars and divalents should be carefully considered as L-GOM may contain high ratio of basal-to-basal/edge-to-basal regions.

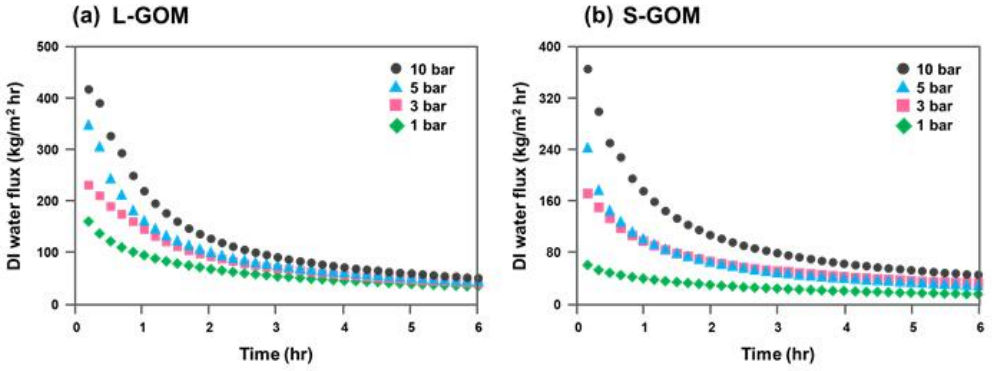


Fig. 4.7. Pure water flux of L-GOM and S-GOM at 1~10bar of pressure

## 4.3 Deposition of $Al_2O_3$ on the GOM by PEALD

An ultra-thin $Al_2O_3$ layer was deposited via ALD based on the TMA reaction with $O_2$ plasma. The formation of the hydroxyl (OH) functional group on the GO membrane via PEALD is explained as follows: (Potts, S E. et al., 2012) and (Langeris, E. et al., 2008) identified the reaction mechanism of ALD-$Al_2O_3$ with Eq. (7) and Eq. (8), respectively:

$$s(-OH)_{ads} + (Al(CH_3)_3) \rightarrow s-OAl(CH_3)_2 + CH_4(g), \quad (7)$$

$$s-OAl(CH_3)_2 + 4O^*(g) \rightarrow s-OAl(OH)_{ads} + H_2O(g) + CO_2(g), \quad (8)$$

where $O^*$ stands for all the $O_2$ plasma induced oxygen species that react with TMA, including $O_2$, O, $O_2^+$, $O^+$, and so on (Langereis, E. et al., 2008). S stands for the substrate and methane ($CH_4$), $H_2O$, and $CO_2$ are by-products of the reaction. In the precursor dosing step, the chemisorption of $Al(CH_3)_3$ occurs at 140℃ at the surface of the GO membrane through a reaction with OH functional groups on the GO (eq. 7). Throughout $O_2$ plasma exposure, oxidation of Al atoms and combustion of the methyl ($CH_3$) functional group occurs by the oxygen

radicals in the plasma. Combustion of $CH_3$ then produces CO, CO, and $H_2O$ (eq. 8). Here, OH surface groups of s-Al(OH) are created by the combustion-like reaction and a reaction with $H_2O$ molecules after $CH_3$ combustion (Heil, S B S., 2008). Thus, the hydroxyl group appears as a consequence of the reaction between the methyl group of TMA and oxygen plasma.

### 4.3.1 Confirmation of ALD-$Al_2O_3$ on the surface of GO membrane

The thickness of the deposited $Al_2O_3$ layer on the GO membrane was estimated using the growth rate of the $Al_2O_3$ layer as a function of high numbers of ALD cycles. Fig. 4.8 shows the thickness of the deposited Al2O3 layer as a function of ALD cycles. Based on the saturation condition of the PEALD cycle, the growth rate of the layer was extracted from the slope of the linear extrapolation of the graph, which was 0.16nm/cycle. Therefore, the thickness of the ultra-thin $Al_2O_3$ layer can be calculated by [number of ALD cycles] × [growth rate: 0.16nm/cycle], and each $Al_2O_3$ layer thickness for 3, 6, and 9 cycles was determined to be approximately 0.48 nm, 0.96 nm, and 1.44 nm, respectively.

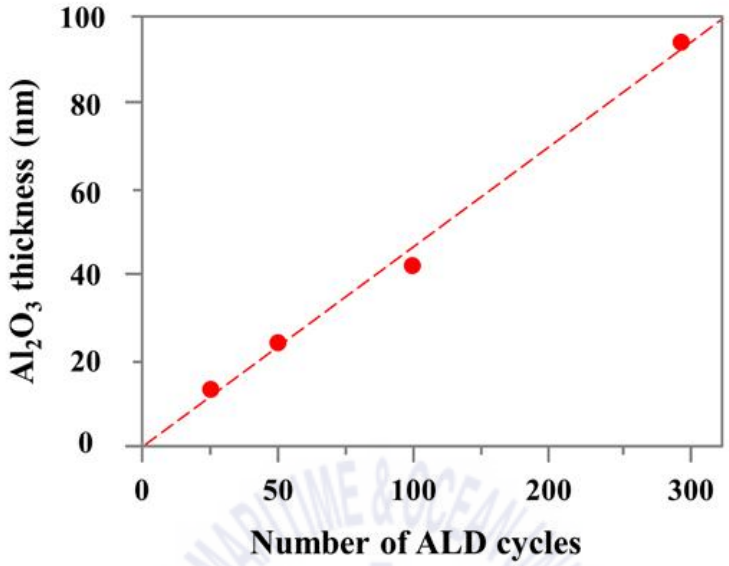


**Fig. 4.8.** The variation of $Al_2O_3$ thickness as a function of ALD cycles.

ALD-$Al_2O_3$ deposition on the GO membrane surface was confirmed by investigating the FESEM (Fig. 4.9a) and EDS analysis (Figs. 4.9b and 4.9c). As can be seen from Fig. 4.9a, the edge of the membrane was selected as an image spot to ensure the alumina deposition on the GO membrane. Figs. 4.9b and 4.9c show the EDS Alk analysis of surface mapping (Fig. 4.9b) and line mapping (Fig. 4.9c), corresponding to the red lined area in Fig. 4.9a. Both figures show that Al was successfully deposited on the GO membrane by PEALD.

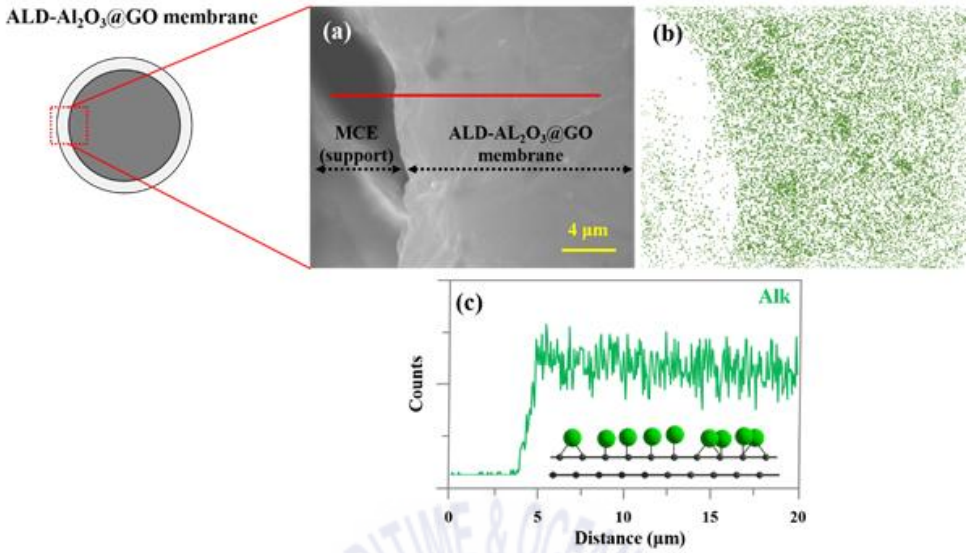


**Fig. 4.9.** (a) FESEM image of the ALD-$Al_2O_3$@GO membrane surface, (b) and (c) EDAX analysis of the ALD-$Al_2O_3$@GO membrane surface. X-axis of (c) represents the distance from the left side of the red colored line in (a) in micrometers

### 4.3.2 Enhanced membrane performance of the ALD-$Al_2O_3$@GOM

In ultra-thin, hydrophilic $Al_2O_3$ layer was deposited on the GO membrane by PEALD in order to overcome reduced salt removal due to the low stability of GO laminar stacked layers on the MCE substrate under aqueous solution. We hypothesized that the ultra-thin hydrophilic surface functionalization via PEALD would not affect hydraulic resistance, but would increase the water affinity of the GO membrane and enhance electrostatic interactions as a salt removal mechanism. Fig. 4.10 represents DI water permeability, NaCl solution permeability, and salt rejection of the as-prepared membranes. Overall, the $Al_2O_3$ deposited GO membrane exhibited an enhanced water permeability and salt rejection. The water permeability of ALD-$Al_2O_3$ (3 cycles) @GO

membrane increased from 39.1LMH/bar to 56.0LMH/bar. This permeability enhancement is consistent with our hypothesis that the functionalization of the GO membrane surface by applying a few cycles of ALD enhances an affinity to water molecules by covering the surface of the membrane. Interestingly, and contrary to the common trade-offs between permeability and selectivity (Geise, G M et al., 2011), salt rejection also increased by 16.9% without losing water and NaCl solution permeability (Fig. 4.10b). One possible explanation for the improvement in both rejection and permeability is that the $Al_2O_3$ functionalized surface of the GO membrane became more hydrophilic than the pristine GO membrane.

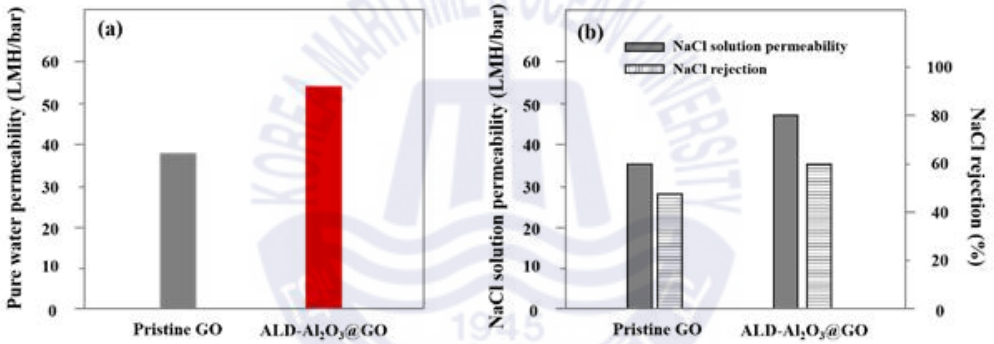


**Fig. 4.10.** Performance of the pristine GO membrane and ALD (monolayer) coated GO membrane (a) pure water permeability and (b) NaCl solution permeability and NaCl rejection.

There are two options for effective pores on the GO membrane for water passage while rejecting larger molecules via the sieving effect (size exclusion): nanopores (defects) on the GO flakes and gaps between each GO flake (You, Y. et al., 2016). Nanopores are considered as undesired defects on 2D graphene and its derivatives in various applications. Karnik et al (2015) noted that these defects on the graphene membranes caused unfavorable salt penetration through the

membrane (O' Hern, S C., 2015). The size of these nanopores also plays a critical role on ion rejection from graphene membranes (O' Hern, S C., 2012; O' Hern, S C., 2014; Nguyen, C. et al., 2018). Considering that few ALD cycles are a solution for healing defective sites on carbon nanomaterials, we may assume that such defects became narrowed with few cycle ALD, and resulted in increased salt rejection. Moreover, it has been reported that the presence of oxygen containing functional groups at the starting point of water pathways in NF and RO membranes increased filtration performance, as it provided the feasibility and affinity of water molecules (Fornasiero, F., 2018; Venvuurt, R H J., 2017; Wenjun, Y. et al., 2018). With ALD-$Al_2O_3$ deposition, the effective pore entrance of the GO membrane increased water affinity to water molecules while being arrowed enough for NaCl rejection. Therefore, in this study, low cycles of ALD-$Al_2O_3$ deposition made the surface of the GO membrane more hydrophilic without pore clogging. This increased surface hydrophilicity resulted in a faster water flux whilst causing differences in solute transport, which consequently increased NaCl retention.

### 4.4 Characterizations of the few cycle ALD-$Al_2O_3$@GO membranes

The physico-chemical properties of the ALD coated GO membranes were investigated to explain the enhanced salt rejection efficiency and water permeability. $Al_2O_3$ layer deposition altered the surface hydrophilicity of the GO membranes. The effect of the ALD on the surface chemistry of the GO membrane was studied by XPS and FT-IR. Fig. 4.11 describes oxygen functional group deposition on the ALD-$Al_2O_3$ treated GO membrane surface. The binding energies of 285.0, 287.1,

288.2 and 288.9eV correspond to C–C, epoxide (C–O), carbonyl (C=O) and carboxylic (O=C–OH), respectively (Fig. 4.10a). Compared to the pristine GO, epoxide peak was decreased only after 3 ALD-$Al_2O_3$ cycles, presumably due to the strong chemical adsorption between oxygenated carbon species and on the GO and TMA (Venvuurt, R H J., 2017). C–C was steadily decreased by increasing ALD cycles up to 9. It indicates $Al_2O_3$ deposition on the GO membrane by the reaction of the TMA precursor with the epoxide group on the GO membrane. Fig. 4.10b shows carbon/oxygen ratio on the ALD treated GO membranes. Atomic concentration of carbon (Fig. 4.10b) reduced from 72.5 to 68.3, 57.3 and 48.2$_{at.}$% for 0, 3, 6 and 9 cycles of ALD, respectively. It indicates that oxygen atom on the GO membrane surface increased as the ALD cycle increased. Thus, we could conclude that ALD-$Al_2O_3$ assisted to coverage of oxygen contents on the carbonic region of GO. To relate the oxygenation of GO surface and enhanced membrane performance, we further examined FT-IR and WCA.

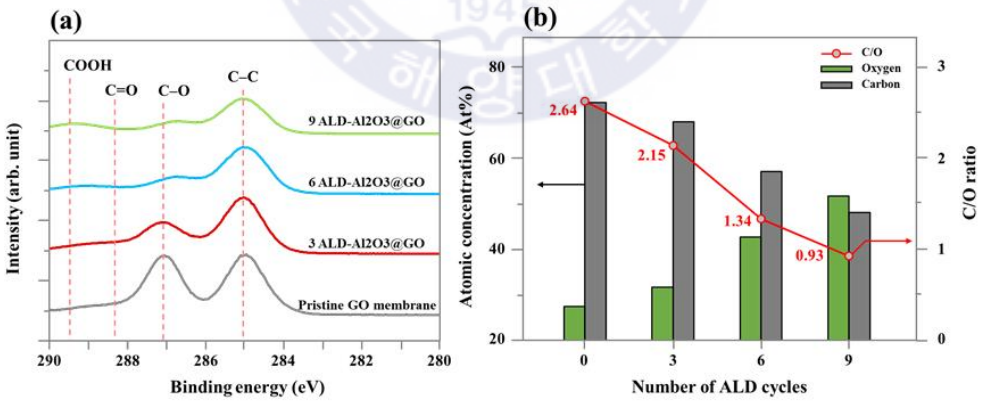


**Fig. 4.11.** (a) XPS spectra and (b) and C/O ratios of the alumina deposited on GO membranes for different ALD cycles

Surface functional group on the surface of the ALD-$Al_2O_3$@GO

membranes was examined by FT-IR. Fig. 4.12 shows the FT-IR spectra of pristine and $Al_2O_3$ deposited GO membranes. The characteristic peak at 1600$cm^{-1}$ of the C=C group and 1160$cm^{-1}$ of the R-O-R group (Wenjun, Y. et al., 2018) disappeared in the FTIR spectrum of 3 ALD cycles on the GO membrane, and was then maintained for 6 and 9 ALD cycles. This is in good accordance with the XPS analysis in Fig. 6a. Moreover, the strength of the peak from 3200$cm^{-1}$ to 3600$cm^{-1}$ of -OH stretching and 1640$cm^{-1}$ of the -OH group increased with the increase in ALD cycles (Marquardt, A E., 2015). It indicates that hydrophilic -OH functional group on the GO surface increased with an increase in the number of ALD cycles.

Surface hydrophilicity of the GO membranes was confirmed by contact angle measurement. Fig. 4.12 shows the water contact angle (WCA) of the ALD treated membranes. It decreased sharply from 84.8° to 58.1° after 3 cycles of $Al_2O_3$ deposition by ALD. Overall, the contact angle displayed a reduced tendency after Al2O3 layer deposition. (Lam, D V., 2014). The ALD-$Al_2O_3$ (3-cycles)@GO membrane was the most hydrophilic, followed by the ALD-Al2O3 (9-cycles)@GO membrane (64.0° ) and ALD-$Al_2O_3$ (6-cycles)@GO membrane (70.7° ). We may assume that the slight increase of WCA over increased ALD cycle is due to the roughened surface (Xie, Q. et al., 2017) by a few cycles of ALD (Lam, D V., 2014; Lee, K. 2012). It is noted that an increase in hydroxyl functional groups on the GO membrane increases water permeability (Yamamoto, K. et al., 2015; Wang, Y. et al., 2017). Therefore, the results of the XPS, FT-IR spectra and water contact angle are in good accordance with the increased performance of water permeability.

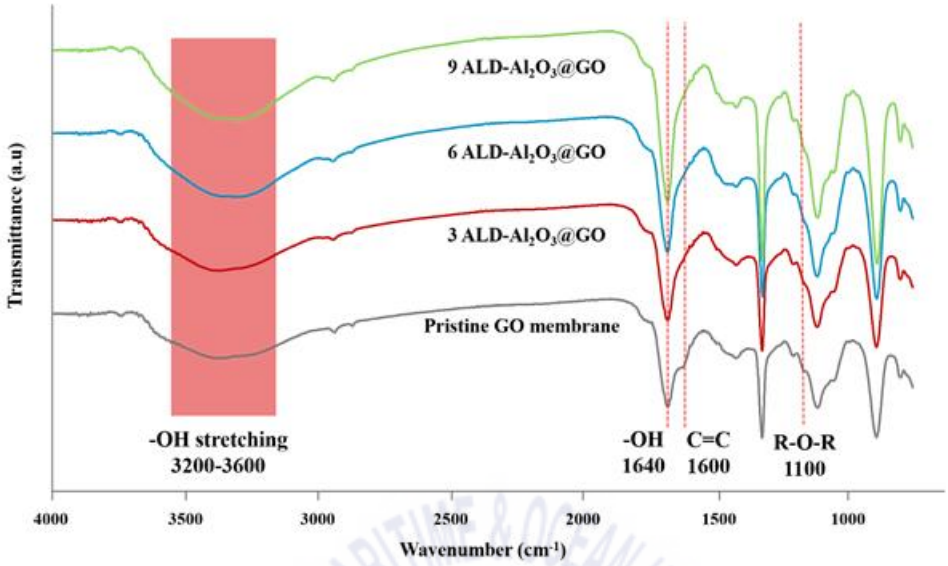


**Fig. 4.12.** FT-IR spectra of the alumina deposited on GO membranes for different ALD cycles

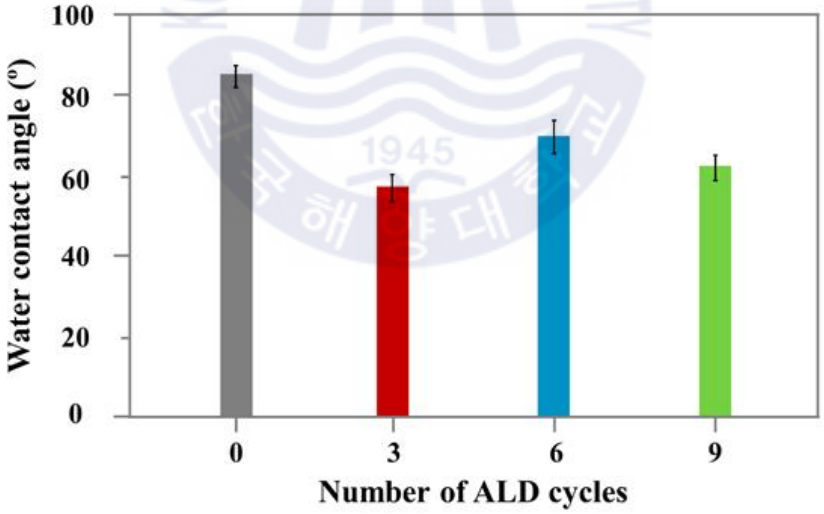


**Fig. 4.13.** Water contact angle measurements for pristine GO membrane and ALD-$Al_2O_3$@GO membranes at various ALD cycles

The effects of ALD on the pore structure of the GO nanochannels were investigated by XRD and Raman measurements. There are two

major pathways of water through multi-layered GO membrane: space between adjacent GO flakes and structural defects of each GO flake. As shown in Fig. 4.15, Overall $Al_2O_3$ deposition via ALD did not change the interlayer spacing between GO nanochannels in both dry and wet conditions. This is because ALD-$Al_2O_3$ mainly contributes to the surface functionalization of the GO membrane and the PEALD process under 140℃ did not affect the GO nanochannels as it was conducted in less than a minute. Under wet conditions, the GO membrane swelled by adsorbing water molecules into the laminarly stacked GO flakes, resulting in an enlarged channel for salt ions to pass through (Zhang, S. 2017; Mi, B S. et al., 2018). This lack of change in the wet state interlayer space in wet conditions may not affect size exclusion by the nanochannels of GO membranes. Moreover, defects on the top GO layer was not changed after the ALD process (Fig. 4.14), showing $I_D/I_G$ ratio of around 1.06 ~ 1.07. It indicates that PEALD process in this study did not alter the structure of GO flake. However, to fully implement ALD process to graphene-based membrane for water treatment, effect of various plasma (e.g., $H_2O$ or HfO) sources and different applied power on the physical properties should be further investigated.

Based on the characterization results, enhanced salt rejection and water permeability was attributed to the excellent uniformity of the $Al_2O_3$ layer with atomic layer thickness via ALD. Overall, hydrophilicity of the modified membranes was increased by ALD-$Al_2O_3$ treatment. This increase in hydrophilicity of the membrane surface is likely due to the increased attachment of the hydrophilic functional group (-OH) on the GO membrane by ALD, as presented by FT-IR results. In addition, the increased water contact angle in ALD treated GO membranes verifies their enhanced water permeability.

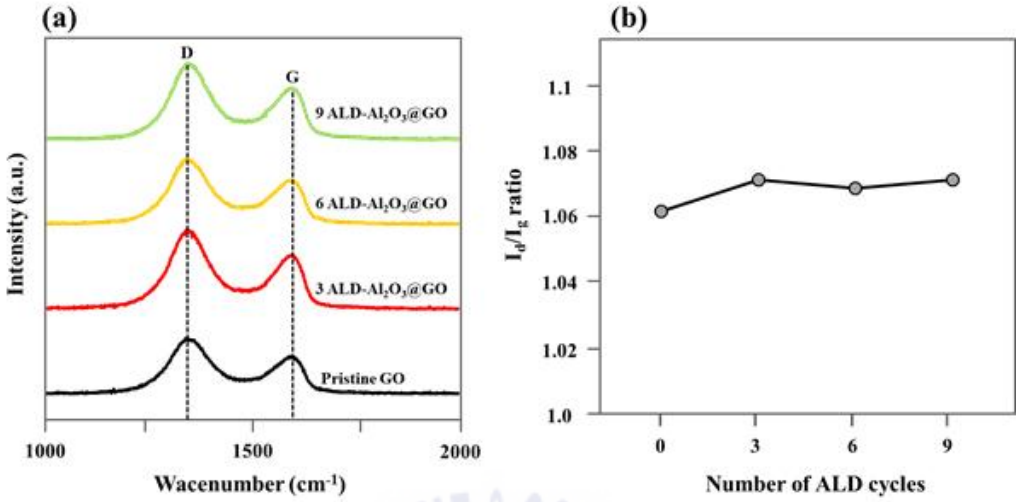


Fig 4.14. Defect configuration of each membranes (a) Raman spectra and (b) $I_D/I_G$ ratio of GO membranes as function of ALD-$Al_2O_3$ cycles

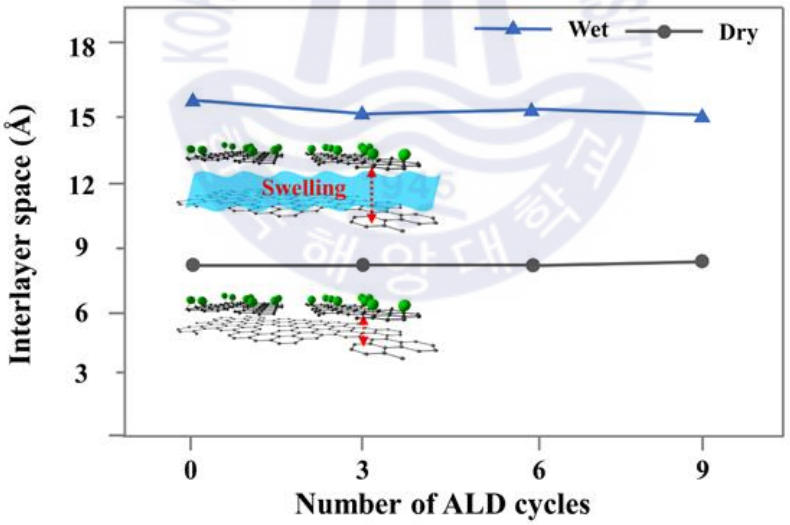


Fig. 4.15. Interlayer space variation of pristine GO membrane and ALD-$Al_2O_3$@GO membranes

## 4.5 Effect of ALD cycles on GOM filtration performance

In order to examine the effect of ALD on enhanced water

permeability and salt rejection, membrane performance as a function of ALD cycles was systematically evaluated using dead-end filtration. It has been reported that applying a different number of ALD cycles to the surface modification alters the pore size, thickness, and hydrophilicity of the membrane that govern the water permeability and selectivity of the membrane (Li, F. et al., 2011; Nikkola, J. et al., 2011; Xu, Q. et al., 2012). The numbers of ALD cycles increased to 3, 6, and 9, which roughly corresponds to the mono layer, bilayer, and tri-layer of $Al_2O_3$ on the GO membrane, respectively. As shown in Fig. 4.16, NaCl solution permeability increased from 54LMH/bar to 72.6LMH/bar with increasing ALD cycles from 3 to 9. Such an enhanced water permeability is attributed to the increase in surface hydrophilicity of the GO membrane with atomic level deposition of the $Al_2O_3$ layer. As shown in the d-space measurement via XRD (Fig. 4.15), the application of up to 9 cycles of ALD did not affect interlayer spacing (d-space) that functions as a water transport channel. Further, the ultra-thin $Al_2O_3$ layer with a thickness of up to 1.44 nm on the GO membrane did not significantly increase the thickness of the GO membrane (GO layer: 10 $\mu$m-20 $\mu$m, MCE: 130 $\mu$m). In this study, ALD mainly increased surface hydrophilicity of the membrane, corresponding to the water contact angle results (Fig. 4.13). This enhanced hydrophilicity is due to the increase in the oxygen containing group (e.g., hydroxyl) on the surface of the membrane with an increase in the number of ALD cycles, as explained in the XPS (Fig. 6) and FT-IR results (Fig. 4.11). In addition, NaCl rejection improved with an increase in the number of ALD cycles. As can be seen in Fig. 4.16, 9 cycles of ALD achieved a 70 % level of salt rejection. Compared to previous studies, the rejection efficiency is comparable to the hydrophilic pDA coated reduced GO membrane (63 %) (Yang, E. et al.,

2018), but is higher than the carbon nanotube (CNT) intercalated GO membrane (51.4 %) (Han, Y. 2015), and the pure GO membrane (35 %). The salt removal mechanism of the laminar stacked GO membrane is based on the combination of size exclusion and electrostatic interaction (Donnan exclusion). Interlayer spacing of the GO flake as a water transport channel is determined by d-space via XRD measurement. Based on MD simulation, optimal interlayer spacing for NaCl size exclusion is reported to be than 0.7 nm due to the size of hydrated Na+ (with a hydrated radius of 0.36 nm) from water. However, as can be seen in XRD analysis (Fig. 4.15), d-space of pristine GO membrane in wet state increased to 1.55 nm from 0.78 nm. It corresponds to the relatively low salt rejection (40 %) of the pristine GO membranes. It indicates that NaCl sieving effect of the GO membrane would be weakened in wet state. Same trend in XRD analysis was observed in the PEALD treated GO membranes. However, salt rejection efficiency was enhanced up to 60 % in the PEALD treated GO membranes. It implies that the main mechanism of salt rejection in ALD-$Al_2O_3$@GO membrane be electrostatic interaction (Donnan exclusion). Rather than improving size exclusion, PEALD contributed to enhancing Donnan exclusion effect by altering surface chemistry of the GO membranes. By increasing the number of ALD cycles up to 9, the hydroxyl group (OH) increased, as represented by the XPS (Fig. 4.11) and FT-IR results (Fig. 4.12). This increase in the negatively charged functional group would increase the surface pore charge of the GO membranes. It is reported that ion rejection in a NF membrane is directly related to the membrane pore charge due to the co-ion electrostatic exclusion (Childress, A E., 2000). Thus, based on the Donnan exclusion model (Pivonka, P. 2007), the more negatively charged GO membrane exhibited enhanced salt rejection.

Based on the density functional theory simulations in previous studies (Vervuurt, R H J. et al., 2017), using TMA as a precursor for $Al_2O_3$ via ALD exhibited strong chemisorption to the hydroxylated GO as compared to the pristine graphene. This is due to the availability of p-orbitals of the surface oxygen on GO reacting with those of the TMA. It subsequently facilitated uniform nucleation and growth for the $Al_2O_3$ layer on the GO substrate (Nourbakhsh, A. et al., 2015)

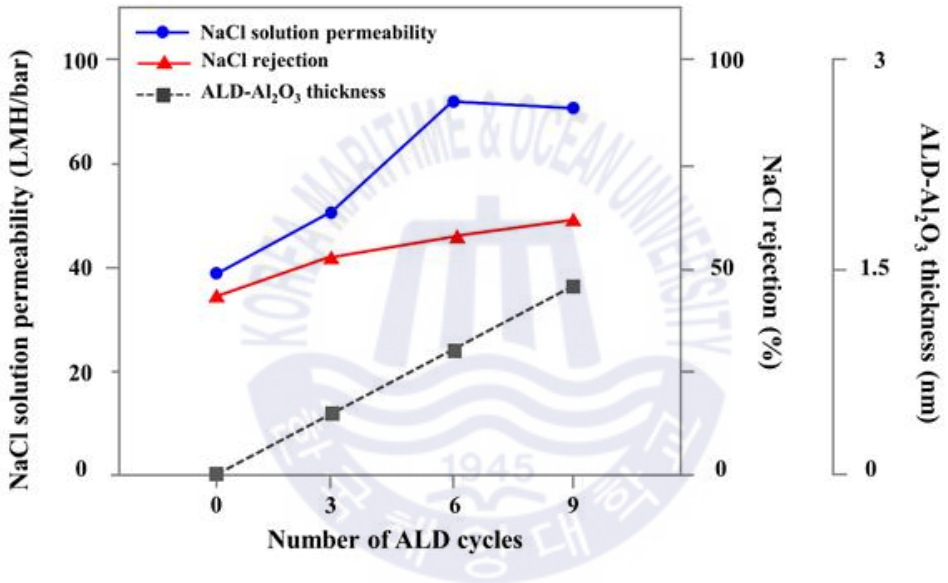


Fig. 4.16. NaCl solution permeability and NaCl rejection performance as a function of different ALD cycles on the GO membrane.

# Chapter 5. Conclusion

In this study, microstructural behavior and sub-nanometer surface functionalization of multi-layered GO membrane were investigated to solve low water permeability and ion rejection. Size-differentiated GO membranes were tested to find optimal size for the water filtration. By destructing GO nano flakes by probe-type sonicator with small energy, mean size and size distribution were greatly declined. However, increase of sonication energy by 5 times showed only mild effect on size decrease. Through XRD analysis of different size GO stacked membranes, S-GOM showed the most disordered and high interlayer space size whilst M-GOM and L-GOM showed relatively regular microstructure under wet state. Invariance microstructure of GO membrane led to dramatic decrease during 6 hours of water filtration regardless of size of GO. The flux decrease rate was much faster for smaller GO stacked membrane due to the enveloped region of GO membranes.

A novel coating method, ALD was implemented to multi-layered GOM. The ALD-$Al_2O_3$@GO membranes had greater water permeability and NaCl rejection than the pristine GO membrane due to the distinctive properties of ALD that functionalizes the surface of the membrane with atomic level functionalization. Based on XRD results, ALD-$Al_2O_3$ deposition did not affect interlayer spacing between GO nanosheets. However, entrance of the GO nanochannel via ALD increased surface hydrophilicity of the GO membrane, leading to enhanced water permeability. By $Al_2O_3$ deposition to the GO membrane surface, -OH bond was provided whilst hindering carbonic region of GO, and

consequently exhibiting improved hydrophilicity. Water permeability increased due to the promoted water affinity to the surface of the GO membrane while salt rejection slightly increased due to the Donnan effects on the GO flake's nanopore. All ALD-$Al_2O_3$@GO membranes exhibited improved performance in NaCl solution permeability.

Therefore, low cycles of ALD-$Al_2O_3$ coating on a GO membrane is considered as a promising modification method for desalination with its atomically thin and uniform coating features. The unique features of ALD enable GO membranes to break the trade-off between permeability and selectivity for water desalination. Moreover, low cycles of ALD can be applied in novel membrane modification with various materials such as titanium (Ti) or silver (Ag).

# References


ALI, S., REHMAN, S. A. U., LUAN, H.-Y., FARID, M. U. & HUANG, H. 2019. Challenges and opportunities in functional carbon nanotubes for membrane-based water treatment and desalination. *Science of The Total Environment,* 646, 1126-1139.

ANAND, A., UNNIKRISHNAN, B., MAO, J.-Y., LIN, H.-J. & HUANG, C.-C. 2018. Graphene-based nanofiltration membranes for improving salt rejection, water flux and antifouling-A review. *Desalination,* 429, 119-133.

BI, R., ZHANG, Q., ZHANG, R., SU, Y. & JIANG, Z. 2018. Thin film nanocomposite membranes incorporated with graphene quantum dots for high flux and antifouling property. *Journal of Membrane Science,* 553, 17-24.

CHILDRESS, A. E. & ELIMELECH, M. 2000. Relating Nanofiltration Membrane Performance to Membrane Charge (Electrokinetic) Characteristics. *Environmental Science & Technology,* 34, 3710-3716.

DREYER, D. R., PARK, S., BIELAWSKI, C. W. & RUOFF, R. S. 2010. The chemistry of graphene oxide. *Chemical Society Reviews,* 39, 228-240.

FORNASIERO, F., PARK, H. G., HOLT, J. K., STADERMANN, M., GRIGOROPOULOS, C. P., NOY, A. & BAKAJIN, O. 2008. Ion exclusion by sub-2-nm carbon nanotube pores. *Proceedings of the National Academy of Sciences,* 105, 17250.

GEISE, G. M., PARK, H. B., SAGLE, A. C., FREEMAN, B. D. & MCGRATH, J. E. 2011. Water permeability and water/salt selectivity tradeoff in polymers for desalination. *Journal of Membrane Science,*

369, 130-138.

GEORGE, S. M. 2010. Atomic Layer Deposition: An Overview. *Chemical Reviews,* 110, 111-131.

GRONER, M. D., FABREGUETTE, F. H., ELAM, J. W. & GEORGE, S. M. 2004. Low-Temperature Al2O3 Atomic Layer Deposition. *Chemistry of Materials,* 16, 639-645.

HAN, Y., JIANG, Y. & GAO, C. 2015. High-Flux Graphene Oxide Nanofiltration Membrane Intercalated by Carbon Nanotubes. *ACS Applied Materials & Interfaces,* 7, 8147-8155.

HEIL, S. B. S., VAN HEMMEN, J. L., VAN DE SANDEN, M. C. M. & KESSELS, W. M. M. 2008. Reaction mechanisms during plasma-assisted atomic layer deposition of metal oxides: A case study for Al2O3. *Journal of Applied Physics,* 103, 103302.

KIM, K., LEE, H.-B.-R., JOHNSON, R. W., TANSKANEN, J. T., LIU, N., KIM, M.-G., PANG, C., AHN, C., BENT, S. F. & BAO, Z. 2014. Selective metal deposition at graphene line defects by atomic layer deposition. *Nature Communications,* 5, 4781.

KIM, S., OU, R., HU, Y., LI, X., ZHANG, H., SIMON, G. P. & WANG, H. 2018. Non-swelling graphene oxide-polymer nanocomposite membrane for reverse osmosis desalination. *Journal of Membrane Science,* 562, 47-55.

LAM, D. V., KIM, S.-M., CHO, Y., KIM, J.-H., LEE, H.-J., YANG, J.-M. & LEE, S.-M. 2014. *Healing defective CVD-graphene through vapor phase treatment.*

LANGEREIS, E., KEIJMEL, J., SANDEN, M. C. M. V. D. & KESSELS, W. M. M. 2008. Surface chemistry of plasma-assisted atomic layer

deposition of Al2O3 studied by infrared spectroscopy. *Applied Physics Letters,* 92, 231904.

LEE, K., JUR, J. S., KIM, D. H. & PARSONS, G. N. 2012. Mechanisms for hydrophilic/hydrophobic wetting transitions on cellulose cotton fibers coated using Al 2 O 3 atomic layer deposition. *Journal of Vacuum Science & Technology A: Vacuum, Surfaces, and Films,* 30, 01a163.

LI, F., LI, L., LIAO, X. & WANG, Y. 2011. Precise pore size tuning and surface modifications of polymeric membranes using the atomic layer deposition technique. *Journal of Membrane Science,* 385-386, 1-9.

LI, N., TIAN, Y., ZHAO, J., ZHANG, J., KONG, L., ZHANG, J. & ZUO, W. 2018. Static adsorption of protein-polysaccharide hybrids on hydrophilic modified membranes based on atomic layer deposition: Anti-fouling performance and mechanism insight. *Journal of Membrane Science,* 548, 470-480.

MARQUARDT, A. E., BREITUNG, E. M., DRAYMAN-WEISSER, T., GATES, G. & PHANEUF, R. J. 2015. Protecting silver cultural heritage objects with atomic layer deposited corrosion barriers. *Heritage Science,* 3, 37.

MI, B. 2014. Graphene Oxide Membranes for Ionic and Molecular Sieving. *Science,* 343, 740-742.

MI, B., ZHENG, S. & TU, Q. 2018. 2D graphene oxide channel for water transport. *Faraday Discussions,* 209, 329-340.

MOHAMMAD, A. W., TEOW, Y. H., ANG, W. L., CHUNG, Y. T., OATLEY-RADCLIFFE, D. L. & HILAL, N. 2015. Nanofiltration membranes review: Recent advances and future prospects. *Desalination,* 356, 226-254.

NGUYEN, C. & BESKOK, A. 2018. *Saltwater transport through pristine*

*and positively charged graphene membranes*.

NIKKOLA, J., SIEV NEN, J., RAULIO, M., WEI, J., VUORINEN, J. & TANG, C. Y. 2014. Surface modification of thin film composite polyamide membrane using atomic layer deposition method. *Journal of Membrane Science,* 450, 174-180.

NOURBAKHSH, A., ADELMANN, C., SONG, Y., LEE, C. S., ASSELBERGHS, I., HUYGHEBAERT, C., BRIZZI, S., TALLARIDA, M., SCHMEI ER, D., VAN ELSHOCHT, S., HEYNS, M., KONG, J., PALACIOS, T. & DE GENDT, S. 2015. Graphene oxide monolayers as atomically thin seeding layers for atomic layer deposition of metal oxides. *Nanoscale,* 7, 10781-10789.

O' HERN, S. C., BOUTILIER, M. S. H., IDROBO, J.-C., SONG, Y., KONG, J., LAOUI, T., ATIEH, M. & KARNIK, R. 2014. Selective Ionic Transport through Tunable Subnanometer Pores in Single-Layer Graphene Membranes. *Nano Letters,* 14, 1234-1241.

O' HERN, S. C., JANG, D., BOSE, S., IDROBO, J.-C., SONG, Y., LAOUI, T., KONG, J. & KARNIK, R. 2015. Nanofiltration across Defect-Sealed Nanoporous Monolayer Graphene. *Nano Letters,* 15, 3254-3260.

O' HERN, S. C., STEWART, C. A., BOUTILIER, M. S. H., IDROBO, J.-C., BHAVIRIPUDI, S., DAS, S. K., KONG, J., LAOUI, T., ATIEH, M. & KARNIK, R. 2012. Selective Molecular Transport through Intrinsic Defects in a Single Layer of CVD Graphene. *ACS Nano,* 6, 10130-10138.

PIVONKA, P., SMITH, D. & GARDINER, B. 2007. Investigation of Donnan equilibrium in charged porous materials - a scale transition analysis. *Transport in Porous Media,* 69, 215-237.

POTTS, S. E., DINGEMANS, G., LACHAUD, C. & KESSELS, W. M. M. 2012. Plasma-enhanced and thermal atomic layer deposition of Al2O3 using dimethylaluminum isopropoxide, [Al(CH3)2(μ-OiPr)]2, as an alternative aluminum precursor. *Journal of Vacuum Science & Technology A,* 30, 021505.

PROFIJT, H. B., POTTS, S. E., SANDEN, M. C. M. V. D. & KESSELS, W. M. M. 2011. Plasma-Assisted Atomic Layer Deposition: Basics, Opportunities, and Challenges. *Journal of Vacuum Science & Technology A,* 29, 050801.

RAJAEIAN, B., RAHIMPOUR, A., TADE, M. O. & LIU, S. 2013. Fabrication and characterization of polyamide thin film nanocomposite (TFN) nanofiltration membrane impregnated with TiO2 nanoparticles. *Desalination,* 313, 176-188.

SHI, W. & PLATA, D. L. 2018. Vertically aligned carbon nanotubes: production and applications for environmental sustainability. *Green Chemistry,* 20, 5245-5260.

SONG, N., GAO, X., MA, Z., WANG, X., WEI, Y. & GAO, C. 2018. A review of graphene-based separation membrane: Materials, characteristics, preparation and applications. *Desalination,* 437, 59-72.

VAN LAM, D., KIM, S.-M., CHO, Y., KIM, J.-H., LEE, H.-J., YANG, J.-M. & LEE, S.-M. 2014. Healing defective CVD-graphene through vapor phase treatment. *Nanoscale,* 6, 5639-5644.

VERVUURT, R. H. J., KARASULU, B., VERHEIJEN, M. A., KESSELS, W. M. M. & BOL, A. A. 2017. Uniform Atomic Layer Deposition of Al2O3 on Graphene by Reversible Hydrogen Plasma Functionalization. *Chemistry of Materials,* 29, 2090-2100.

WANG, X., TABAKMAN, S. M. & DAI, H. 2008. Atomic Layer Deposition of Metal Oxides on Pristine and Functionalized Graphene. *Journal of the American Chemical Society,* 130, 8152-8153.

WANG, Y., HE, Z., GUPTA, K. M., SHI, Q. & LU, R. 2017. Molecular dynamics study on water desalination through functionalized nanoporous graphene. *Carbon,* 116, 120-127.

WEI, Y., ZHANG, Y., GAO, X., MA, Z., WANG, X. & GAO, C. 2018. Multilayered graphene oxide membrane for water treatment: A review. *Carbon,* 139, 964-981.

WENJUN, Y., DU, C., SHEN, Y.-Z. & JIANMIN, Z. 2018. *Application of Graphene-Oxide-Modified Polyacrylate Polymer for Controlled-Release Coated Urea*.

XIE, Q., SHAO, W., ZHANG, S., HONG, Z., WANG, Q. & ZENG, B. 2017. Enhancing the performance of thin-film nanocomposite nanofiltration membranes using MAH-modified GO nanosheets. *RSC Advances,* 7, 54898-54910.

XU, Q., YANG, Y., WANG, X., WANG, Z., JIN, W., HUANG, J. & WANG, Y. 2012. Atomic layer deposition of alumina on porous polytetrafluoroethylene membranes for enhanced hydrophilicity and separation performances. *Journal of Membrane Science,* 415-416, 435-443.

YAMAMOTO, K., OHSHITA, J., MIZUMO, T., KANEZASHI, M. & TSURU, T. 2015. Preparation of hydroxyl group containing bridged organosilica membranes for water desalination. *Separation and Purification Technology,* 156, 396-402.

YANG, E., ALAYANDE, A. B., KIM, C.-M., SONG, J.-H. & KIM, I. S.

2018. Laminar reduced graphene oxide membrane modified with silver nanoparticle-polydopamine for water/ion separation and biofouling resistance enhancement. *Desalination,* 426, 21-31.

YANG, E., KIM, C.-M., SONG, J.-H., KI, H., HAM, M.-H. & KIM, I. S. 2017a. Enhanced desalination performance of forward osmosis membranes based on reduced graphene oxide laminates coated with hydrophilic polydopamine. *Carbon,* 117, 293-300.

YANG, L., WANG, Z. & ZHANG, J. 2017b. Highly permeable zeolite imidazolate framework composite membranes fabricated via a chelation-assisted interfacial reaction. *Journal of Materials Chemistry A,* 5, 15342-15355.

YOU, Y., SAHAJWALLA, V., YOSHIMURA, M. & JOSHI, R. K. 2016. Graphene and graphene oxide for desalination. *Nanoscale,* 8, 117-119.

ZHANG, Y. & CHUNG, T.-S. 2017. Graphene oxide membranes for nanofiltration. *Current Opinion in Chemical Engineering,* 16, 9-15.

ZHENG, S., TU, Q., URBAN, J. J., LI, S. & MI, B. 2017. Swelling of Graphene Oxide Membranes in Aqueous Solution: Characterization of Interlayer Spacing and Insight into Water Transport Mechanisms. *ACS Nano,* 11, 6440-6450.

ZHOU, D., ZHU, L., FU, Y., ZHU, M. & XUE, L. 2015. Development of lower cost seawater desalination processes using nanofiltration technologies — A review. *Desalination,* 376, 109-116.

ZHOU, X., ZHAO, Y.-Y., KIM, S.-R., ELIMELECH, M., HU, S. & KIM, J.-H. 2018. Controlled TiO2 Growth on Reverse Osmosis and Nanofiltration Membranes by Atomic Layer Deposition: Mechanisms and Potential Applications. *Environmental Science & Technology,* 52,

14311-14320.

AKBARI, A., SHEATH, P., MARTIN, S. T., SHINDE, D. B., SHAIBANI, M., BANERJEE, P. C., TKACZ, R., BHATTACHARYYA, D. & MAJUMDER, M. 2016. Large-area graphene-based nanofiltration membranes by shear alignment of discotic nematic liquid crystals of graphene oxide. *Nature Communications,* 7, 10891.

AN, D., YANG, L., WANG, T.-J. & LIU, B. 2016. Separation Performance of Graphene Oxide Membrane in Aqueous Solution. *Industrial & Engineering Chemistry Research,* 55, 4803-4810.

BORETTI, A., AL-ZUBAIDY, S., VACLAVIKOVA, M., AL-ABRI, M., CASTELLETTO, S. & MIKHALOVSKY, S. 2018. Outlook for graphene-based desalination membranes. *npj Clean Water,* 1, 5.

CHEN, B., JIANG, H., LIU, X. & HU, X. 2017. Molecular Insight into Water Desalination across Multilayer Graphene Oxide Membranes. *ACS Applied Materials & Interfaces,* 9, 22826-22836.

CHEN, J., LI, Y., HUANG, L., JIA, N., LI, C. & SHI, G. 2015. Size Fractionation of Graphene Oxide Sheets via Filtration through Track-Etched Membranes. *Advanced Materials,* 27, 3654-3660.

CHONG, J. Y., WANG, B., MATTEVI, C. & LI, K. 2018. Dynamic microstructure of graphene oxide membranes and the permeation flux. *Journal of Membrane Science,* 549, 385-392.

CHU, K. H., HUANG, Y., YU, M., HER, N., FLORA, J. R. V., PARK, C. M., KIM, S., CHO, J. & YOON, Y. 2016. Evaluation of Humic Acid and Tannic Acid Fouling in Graphene Oxide-Coated Ultrafiltration Membranes. *ACS Applied Materials & Interfaces,* 8, 22270-22279.

DOLBIN, A. V., KHLISTYUCK, M. V., ESEL'SON, V. B., GAVRILKO, V. G.,

VINNIKOV, N. A., BASNUKAEVA, R. M., MALUENDA, I., MASER, W. K. & BENITO, A. M. 2016. The effect of the thermal reduction temperature on the structure and sorption capacity of reduced graphene oxide materials. *Applied Surface Science,* 361, 213-220.

GON ALVES, G., VILA, M., BDIKIN, I., DE ANDR S, A., EMAMI, N., FERREIRA, R. A. S., CARLOS, L. D., GR CIO, J. & MARQUES, P. A. A. P. 2014. Breakdown into nanoscale of graphene oxide: Confined hot spot atomic reduction and fragmentation. *Scientific Reports,* 4, 6735.

HUANG, D., WU, J., WANG, L., LIU, X., MENG, J., TANG, X., TANG, C. & XU, J. 2019. Novel insight into adsorption and co-adsorption of heavy metal ions and an organic pollutant by magnetic graphene nanomaterials in water. *Chemical Engineering Journal,* 358, 1399-1409.

HUANG, L., ZHANG, M., LI, C. & SHI, G. 2015. Graphene-Based Membranes for Molecular Separation. *The Journal of Physical Chemistry Letters,* 6, 2806-2815.

KIM, S., OU, R., HU, Y., LI, X., ZHANG, H., SIMON, G. P. & WANG, H. 2018. Non-swelling graphene oxide-polymer nanocomposite membrane for reverse osmosis desalination. *Journal of Membrane Science,* 562, 47-55.

KLECHIKOV, A., YU, J., THOMAS, D., SHARIFI, T. & TALYZIN, A. V. 2015. Structure of graphene oxide membranes in solvents and solutions. *Nanoscale,* 7, 15374-15384.

LE, G. T. T., CHANLEK, N., MANYAM, J., OPAPRAKASIT, P., GRISDANURAK, N. & SREEARUNOTHAI, P. 2019. Insight into the ultrasonication of graphene oxide with strong changes in its properties and performance for adsorption applications. *Chemical Engineering*

*Journal,* 373, 1212-1222.

MEDHEKAR, N. V., RAMASUBRAMANIAM, A., RUOFF, R. S. & SHENOY, V. B. 2010. Hydrogen Bond Networks in Graphene Oxide Composite Paper: Structure and Mechanical Properties. *ACS Nano,* 4, 2300-2306.

MI, B., ZHENG, S. & TU, Q. 2018. 2D graphene oxide channel for water transport. *Faraday Discussions,* 209, 329-340.

MOON, I. K., LEE, J., RUOFF, R. S. & LEE, H. 2010. Reduced graphene oxide by chemical graphitization. *Nature Communications,* 1, 73.

NAIR, R. R., WU, H. A., JAYARAM, P. N., GRIGORIEVA, I. V. & GEIM, A. K. 2012. Unimpeded Permeation of Water Through Helium-Leak-Tight Graphene-Based Membranes. *Science,* 335, 442-444.

QI, G.-Q., CAO, J., BAO, R.-Y., LIU, Z.-Y., YANG, W., XIE, B.-H. & YANG, M.-B. 2013. Tuning the structure of graphene oxide and the properties of poly(vinyl alcohol)/graphene oxide nanocomposites by ultrasonication. *Journal of Materials Chemistry A,* 1, 3163-3170.

QI, H., LI, Z., TAO, Y., ZHAO, W., LIN, K., NI, Z., JIN, C., ZHANG, Y., BI, K. & CHEN, Y. 2018. Fabrication of sub-nanometer pores on graphene membrane for ion selective transport. *Nanoscale,* 10, 5350-5357.

SARASWAT, V., JACOBBERGER, R. M., OSTRANDER, J. S., HUMMELL, C. L., WAY, A. J., WANG, J., ZANNI, M. T. & ARNOLD, M. S. 2018. Invariance of Water Permeance through Size-Differentiated Graphene Oxide Laminates. *ACS Nano,* 12, 7855-7865.

SHEN, B., ZHAI, W., LU, D., WANG, J. & ZHENG, W. 2012. Ultrasonication-assisted direct functionalization of graphene with macromolecules. *RSC Advances,* 2, 4713-4719.

STOBINSKI, L., LESIAK, B., MALOLEPSZY, A., MAZURKIEWICZ, M., MIERZWA, B., ZEMEK, J., JIRICEK, P. & BIELOSHAPKA, I. 2014. Graphene oxide and reduced graphene oxide studied by the XRD, TEM and electron spectroscopy methods. *Journal of Electron Spectroscopy and Related Phenomena,* 195, 145-154.

TALYZIN, A. V., HAUSMANINGER, T., YOU, S. & SZAB , T. 2014. The structure of graphene oxide membranes in liquid water, ethanol and water-ethanol mixtures. *Nanoscale,* 6, 272-281.

WEI, Y., ZHANG, Y., GAO, X., YUAN, Y., SU, B. & GAO, C. 2016. Declining flux and narrowing nanochannels under wrinkles of compacted graphene oxide nanofiltration membranes. *Carbon,* 108, 568-575.

XIA, M.-Y., XIE, Y., YU, C.-H., CHEN, G.-Y., LI, Y.-H., ZHANG, T. & PENG, Q. 2019. Graphene-based nanomaterials: the promising active agents for antibiotics-independent antibacterial applications. *Journal of Controlled Release,* 307, 16-31.

YANG, E., ALAYANDE, A. B., KIM, C.-M., SONG, J.-H. & KIM, I. S. 2018a. Laminar reduced graphene oxide membrane modified with silver nanoparticle-polydopamine for water/ion separation and biofouling resistance enhancement. *Desalination,* 426, 21-31.

YANG, E., HAM, M.-H., PARK, H. B., KIM, C.-M., SONG, J.-H. & KIM, I. S. 2018b. Tunable semi-permeability of graphene-based membranes by adjusting reduction degree of laminar graphene oxide layer. *Journal of Membrane Science,* 547, 73-79.

ZHANG, T., ZHU, G.-Y., YU, C.-H., XIE, Y., XIA, M.-Y., LU, B.-Y., FEI, X. & PENG, Q. 2019. The UV absorption of graphene oxide is size-dependent: possible calibration pitfalls. *Microchimica Acta,* 186.

ZHAO, Y., LI, C., FAN, X., WANG, J., YUAN, G., SONG, X., CHEN, J. & LI, Z. 2016. Study on the separation performance of the multi-channel reduced graphene oxide membranes. *Applied Surface Science,* 384, 279-286.

ZHENG, S., TU, Q., URBAN, J. J., LI, S. & MI, B. 2017. Swelling of Graphene Oxide Membranes in Aqueous Solution: Characterization of Interlayer Spacing and Insight into Water Transport Mechanisms. *ACS Nano,* 11, 6440-6450.

# Academic achievement

## Peer-reviewed journal article (International)

1. Wan-Cheol Cho, Kyung-Min Poo, Hend Omar Mohamed, **Tae-Nam Kim**, Yul-Seong Kim, Moon Hyun Hwang, Do-Won Jung and Kyu-Jung Chae. "Non-Selective Rapid Electro-Oxidation of Persistent, Refractory Vocs in Industrial Wastewater Using a Highly Catalytic and Dimensionally Stable Ir-pd/Ti Composite Electrode." *Chemosphere* 206, (2018): 483-490.

## Peer-reviewed journal article (Domestic)

1. 조완철, 부경민, 이지은, **김태남**, 채규정, "전극의 부반응 기포발생에 따른 휘발특성과 전기화학고도산화능을 동시에 고려한 휘발성 유기화합물 처리용 최적 불용성전극 개발", 대한상하수도학회, (2019)

## Conference presentations (International)

1. **Tae-Nam Kim**, Jieun Lee, Moon-Hyun Hwang, Kyoung-Hoon Chu, Kyu-Jung Chae, Water / ion separation & filtration performance of multi-layered graphene oxide membrane depending on the controlled graphene oxide flake size, PERMEA 2019 Membrane Conference of Visegrad Countries, Budapest, Hungary, 26-29, Aug, 2019.2.
2. **Tae-Nam Kim**, Jieun Lee, Ji-Hoon Ahn, Kyu-Jung Chae, Tailoring sub-nanometer coating on graphene oxide membrane by atomic layer deposition for enhanced desalination performance, PERMEA 2019 Membrane Conference of Visegrad Countries, Budapest, Hungary, 26-29, Aug, 2019.3.
3. **Tae-Nam Kim**, Ji-Hoon Ahn, Ju-Eun Lee, In-Soo Kim, Kyu-Jung Chae, Surface Modification of Graphene Oxide Membrane for Seawater

Desalination by Atomic Layer Deposition, *2018 Asia Pacific Society of Materials Research*, Sapporo, Japan, 19-22, Jul, 2018.4.

4. Wan-Cheol Cho, **Tae-Nam Kim**, Kyung-Rok Kim, Kyung-Min Poo, In-Soo Kim, Do-Won Jung and Kyu-Jung Chae, Evaluation of VOCs removal performance using anodic oxidation with various platinum group catalysts, *2017 International Environmental Engineering Conference and Annual Meeting of the Korean Society of Environmental Engineers (IEEC 2017),* Jeju, Korea, 15-17, Nov, 2017, p.255-256.5.
5. Wan-Cheol Cho, Kyung-Min Poo, **Tae-Nam Kim**, In-Soo Kim and Kyu-Jung Chae, Selection of suitable electrode for 1,4-dioxane wastewater treatment using DSAs and BDD electrode, *Asia Pacific Society for Materials Research 2018 Annual Meeting (APSMR 2018 Annual Meeting)*, Hokkaido, Japan, 19-22 Jul, 2018.

## Conference presentations (Domestic)

1. **Tae-Nam Kim**, Ji-Hoon Ahn, Ji-Eun Lee, Jae-Soo Chang, In-Soo Kim, Kyu-Jung Chae, Enhancing water desalination performance of multi-layered graphene oxide membrane using atomic layer deposition, 2018 대한환경공학회, 광주, 대한민국, 2018.
2. 조완철, **김태남**, 김동수, 김경록, 손은비, 부경민, 채규정, 친환경응집제와 미세기포를 이용한 2단막 배출수 부상분리특성 연구, 2016 대한환경공학회, 경주, 대한민국, 16-18 Nov, 2016, p.409-410.
3. 김동수, 안창효, 채규정, 조완철, 김태남, 김경록, 이용수, 멀티보어형 분리막을 이용한 2단 막여과 공정에서 여과특성 연구, 2016 대한환경공학회, 경주, 대한민국, 16-18 Nov, 2016, p.407-408.
4. 조완철, 박성관, **김태남**, 부경민, 채규정, 복합촉매 DSA 전극을 이용한 유류폐수의 전기화학고도산화 처리, 2017 한국물환경학회, 광주, 대한민국, 23-24 Mar, 2017, p.755-756.

5. 조완철, 박성관, **김태남**, 부경민, 채규정, 복합촉매 DSA 전극을 이용한 유류폐수의 전기화학고도산화 처리, 대한상하수도학회• 한국물환경학회 2017년 공동학술발표회, 광주, 대한민국, 23-24 Mar, 2017, p.755-756.
6. 조완철, **김태남**, 부경민, 김인수, 장재수, 채규정, BDD 전극과 복합촉매 DSA 전극을 이용한 1,4-다이옥산 함유폐수의 전기화학고도산화 처리, 한국물환경학회•대한상하수도학회 2018년 공동학술발표회, 일산, 대한민국, 22-23 Mar, 2017, p.192-193.
7. **김태남**, 조완철, 부경민, 김인수, 장재수, 채규정, 유해화학물질이 함유된 유류폐수의 급속처리를 위한 DSA와 BDD 전극의 적용 및 평가, 한국물환경학회•대한상하수도학회 2018년 공동학술발표회, 일산, 대한민국, 22-23 Mar, 2017, p.297-298.
8. 조완철, **김태남**, 부경민, 손은비, 김인수, 채규정, 1,4-다이옥산 함유폐수의 전기화학적 고도산화 처리를 위한 Boron-doped diamond 전극과 Dimensionally stable anode의 특성 평가, 2018 대한환경공학회, 광주, 대한민국, 14-16 Nov, p.259-260.

## Awards

1. Student Poster Award, **Tae-Nam Kim**, Jieun Lee, Moon-Hyun Hwang, Kyoung-Hoon Chu, Kyu-Jung Chae , Water / ion separation & filtration performance of multi-layered graphene oxide membrane depending on the controlled graphene oxide flake size, PERMEA 2019 Membrane Conference of Visegrad Countries, Budapest, Hungary, 26-29, Aug, 2019.
2. 학술연구발표회논문상, 조완철, **김태남**, 김동수, 김경록, 손은비, 부경민, 채규정, 친환경응집제와 미세기포를 이용한 2단막 배출수 부상분리특성 연구, 2017 대한환경공학회 국내학술대회, 제주, 대한민국, 15-17, Nov, 2017.